GEOLOGICA CARPATHICA, 2025, 76, 2, 93–116 https://doi.org/10.31577/GeolCarp.2025.05

Evolution of the Štiavnica Stratovolcano revisited: SHRIMP U–Th–Pb zircon dating of subvolcanic intrusions, caldera fill and B. Hodruša precious/base metal deposit (including Re/Os and K/Ar data)

JAROSLAV LEXA[1,✉], KEEWOOK YI[2], IGOR BROSKA[1], ZUZANNA CIESIELSKA[3], PETER KODĚRA[4], MILAN KOHÚT[1], RYAN MATHUR[5], JÁN PRCÚCH[6], MAREK SZCZERBA[3], PETER UHLÍK[4] and RASTISLAV VOJTKO[7]

[1]Earth Science Institute of the Slovak Academy of Sciences, Dúbravská cesta 9, 840 05 Bratislava, Slovakia
[2]Division of Earth and Environmental Sciences, Ochang Center, Korea Basic Science Institute, Chungbuk 28119, Republic of Korea
[3]Institute of Geological Sciences, Polish Academy of Sciences – Research Centre in Cracow, ul. Senacka 1, 31-002 Kraków, Poland
[4]Department of Mineralogy, Petrology and Economic Geology, Faculty of Natural Sciences, Comenius University, Ilkovičova 6, 842 15 Bratislava, Slovakia
[5]Department of Geology, Juniata College, Huntingdon, PA 16652, USA
[6]Slovenská Banská, Ltd., 966 61 Hodruša-Hámre 388, Slovakia
[7]Department of Geology and Paleontology, Faculty of Natural Sciences, Comenius University, Ilkovičova 6, 842 15 Bratislava, Slovakia

(Manuscript received November 5, 2024; accepted in revised form June 11, 2025; Associate Editor: Lukáš Krmíček)

Abstract: A general timing of the Štiavnica Stratovolcano edifice evolution based on structural relationships, biostratigraphic data and previous dating by K/Ar and Rb/Sr methods could not resolve more exactly the critical interval of the subvolcanic intrusive complexes emplacement, a caldera subsidence and evolution of related mineralizations. To fill the gap we have carried out 20 precise SHRIMP U–Th–Pb zircon datings of relevant intrusive and volcanic rocks as well as K/Ar dating of illite and adularia and Re/Os dating of gold and sulfides from a related epithermal mineralization. Their high precision allowed to recognize a succession of subvolcanic intrusions concluded by the caldera collapse and to establish age of the B. Hodruša precious/base metal epithermal mineralization. Based on new interpreted age intervals for individual stages and sub-stages in a complex evolution of the Štiavnica Stratovolcano edifice we update the scheme of its evolution as follows: (1) construction of an extensive and complex andesite stratovolcanic edifice during the interval 15.0–13.6 Ma, including emplacement of a diorite intrusion around 14.8 Ma and emplacement of a diorite porphyry stock at Beluj 14.5 Ma; (2) emplacement of subvolcanic intrusive rocks including: emplacement of rare quartz-diorite porphyry sills pre-dating the B. Hodruša epithermal mineralization around 13.6 Ma; emplacement of the granodiorite bell-jar pluton around 13.44 Ma; granodiorite pluton resurgent uplift, sector collapse and related evolution of the B. Hodruša epithermal mineralization in the interval of ca. 13.44–13.31 Ma; emplacement of quartz-diorite sills in the shear zone that post-date the epithermal mineralization around 13.31 Ma; emplacement of other quartz-diorite porphyry sills and ring dikes during the interval of ca. 13.3–13.0 Ma; emplacement of granodiorite porphyry stocks and dike clusters around 12.9 Ma; (3) subsidence of the caldera and its filling by evolved andesites around 12.9 Ma; (4) renewed activity of less evolved and mixed type andesites during the interval of ca. 12.8–12.3 Ma; (5) uplift of the resurgent horst in the central part of the caldera accompanied by rhyolite volcanic/intrusive activity between 12.3 and 11.4 Ma.

Keywords: Štiavnica Stratovolcano edifice, structure, evolution, U–Th–Pb zircon dating

We dedicate this contribution to the late RNDr. Vlastimil Konečný, CSc., who played a leading role in mapping of the Štiavnica Stratovolcano and along with J. Lexa has laid down essential aspects of its geology and evolution.

Introduction

The Štiavnica Stratovolcano edifice is the most extensive one among the Miocene to Quaternary volcanoes of the Carpathian–Pannonian region that hosts the world-class Banská Štiavnica ore district with exploited reserves estimated at 90 tons of gold, 4000 tons of silver, 70,000 t of Zn, 55,000 t of Pb and 8000 t of Cu (Lexa et al. 1999a + production during last 25 years). It has well-preserved volcanic complexes that allowed a detailed paleovolcanic reconstruction (Konečný et al. 1998a; Chernyshev et al. 2013), while a resurgent horst in the central part of its caldera exposes subvolcanic intrusive complexes and related ore mineralizations. Thanks to a detailed geological mapping, extensive past and ongoing mining works, exploration drilling and laboratory investigation of variable mineralization types there exists a comprehensive data set concerning their geological setting. In addition, recent studies enabled recognition of a resurgent uplift and

✉ corresponding author: Jaroslav Lexa
jaroslav.lexa@savba.sk

a sector collapse structures (contemporaneous with the evolution of the subvolcanic intrusive complex) that host the B. Hodruša epithermal mineralization in its basal shear zone (Kubač et al. 2018). Structural relationships, biostratigraphic data and previous dating by K/Ar and Rb/Sr methods established a general timing of the Štiavnica Stratovolcano edifice evolution (Chernyshev et al. 2013 and references therein). However, it could not resolve more exactly the critical interval of the subvolcanic intrusive complexes emplacement and a caldera subsidence due to a rather low precision of conventional K/Ar and Rb/Sr methods as well as their limits in the area that has been affected by a regional propylitic alteration with a probable rejuvenation of relevant isotopic systems. In this work we present newly acquired results of precise SHRIMP U–Th–Pb zircon dating applied to subvolcanic intrusions and caldera filling that enabled to complete the story. An attempt has been also made to date the contemporaneous epithermal mineralization by the K/Ar method applied to illite and adularia and the Re/Os method applied to gold and sulfides. New results enable an essential reinterpretation of the Štiavnica Stratovolcano edifice evolution including its subvolcanic intrusions and related metallogenetic processes. The work represents an update to incomplete preliminary results published by Lexa et al. (2019). Along with data on magmatic evolution of the stratovolcano (Rotier et al. 2020) and genesis of related mineralizations (Koděra et al. 2004, 2005, 2010, 2014, 2021, 2023; Kozák et al. 2017; Kubač et al. 2018) this work opens a way to a fundamental discussion of mutual relationships among magmatic, structural and metallogenetic processes in large and complex andesitic volcanic edifices.

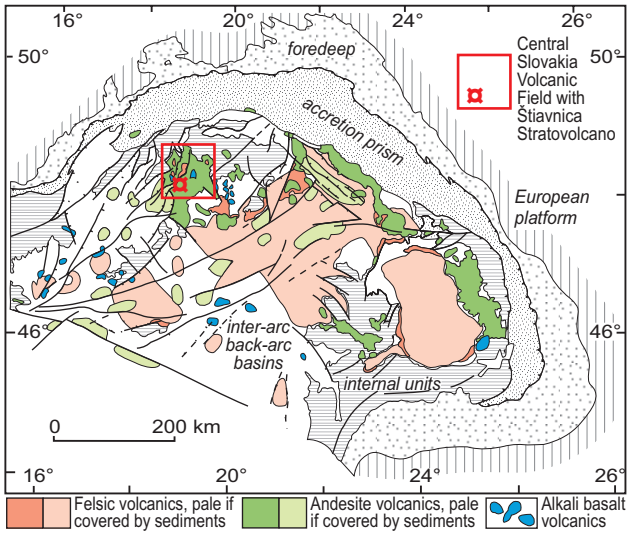

Fig. 1. Position of the Central Slovakia Volcanic Field and Štiavnica Stratovolcano edifice in the structural framework of the Carpathian arc and Pannonian Basin. Modified after Pécskay et al. (2006).

Geological setting

The Central Slovakia Volcanic Field (CSVF), including the Štiavnica Stratovolcano edifice, represents a part of the widespread Miocene to Quaternary volcanic formations in the Carpathian–Pannonian region (Fig. 1). During the Miocene to Quaternary the Carpathian orogenic arc in the northern branch of the Alpine belt in Europe involved older Variscan/Alpine continental crust of the Alcapa and Tisia (Tisza)–Dacia microplates. The orogenic arc migrated northward, northeastward and eastward due to a subduction of oceanic and suboceanic crust of fore-arc flysch basins until it collided with the margin of the European Platform. Sediments of the fore-arc flysch basins were converted into a thrust and fault belt of the accretion prism with a foredeep at its front. The orogenic arc retreat into the area of former flysch basins was compensated by formation of inter-arc and back-arc extensional basins (e.g., Czontos et al. 1992; Nemčok et al. 1998; Konečný et al. 2002; Seghedi & Downes 2011).

Volcanic activity was closely related to the tectonic evolution of the region. Harangi et al. (2024) provide a comprehensive review of relationships and relevant processes. An interplay of subduction, slab break-of associated with an arc-continent colission and back- and inter-arc extension with related asthenosphere upwelling created conditions for generation of a diverse suites of volcanic rocks, namely the calc-alkaline, K-alkalic (shoshonitic), ultra-K and Na-alkalic magma types that reflect a composition of their sources (asthenosphere, mantle lithosphere and/or crust). While the decompression partial melting of asthenosphere followed by an interaction of melts with mantle lithosphere gave rise to K-alkaline, ultra-K and Na-alkaline magmas, extension-related decompression and associated tectonothermal rejuvenation affecting metasomatized mantle lithosphere gave rise to calc-alkaline water-bearing mafic magmas (e.g., Lexa & Konečný 1988; Harangi et al. 2007; Seghedi & Downes 2011) that further evolved towards silicic and/or andesitic magmas in a deep crustal hot zone at the base of lower crust by mixing, assimilation, storage and hybridization (MASH – cf. Hildreth & Moorbath 1988; Annen et al. 2006).

The CSVF extends over 5000 km^2 in the area of Inner Western Carpathians (Fig. 1). Principal units of pre-volcanic basement comprise Variscan granitoids and crystalline shists with their Late Paleozoic to Early Cretaceous sedimentary cover that are defined as thick-skinned crustal sheets tectonically juxtaposed through north-directed thrusting during the early Late Cretaceous time (Andrusov 1968). The CSVF consists of 11 andesitic complex/compound or simple volcanoes and subordine rhyodacite/rhyolite volcanic formations (Fig. 2) that evolved in close spatial and temporal relationships with a horst/graben structure owing to a contemporaneous back-arc extension (Konečný et al. 1995; Lexa & Konečný 1988). Chemical composition of the CSVF rocks points to their calc-alkaline trend of the medium- to high-K type (Lexa & Konečný 1988). A thorough petrological analysis has confirmed that a complex evolution of the Štiavnica Stratovolcano edifice reflected a complex and protracted evolution of a trans-crustal magmatic system with most of the intrusive and

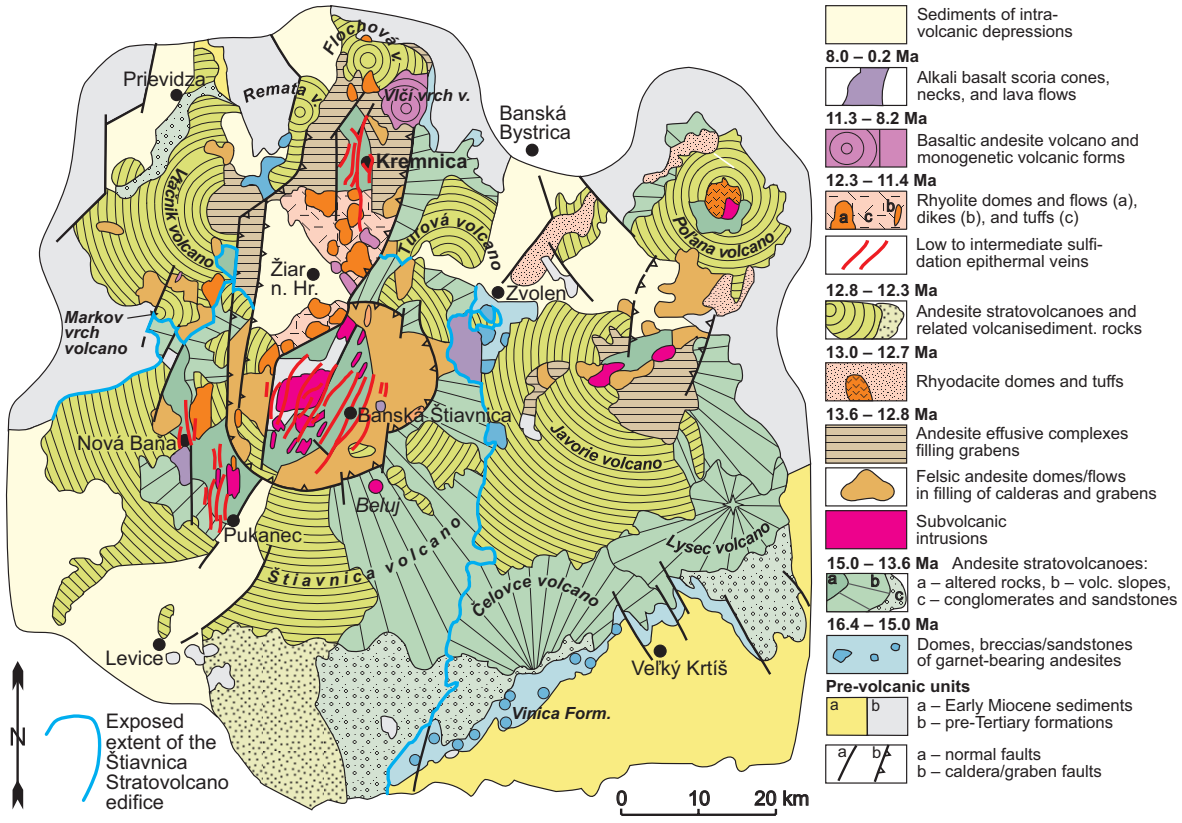

Fig. 2. Extent of the Štiavnica Stratovolcano edifice in the structural scheme of the Middle to Upper Miocene Central Slovakia Volcanic Field. Time intervals in the legend are based especially on results from the Štiavnica Stratovolcano edifice, including those in this paper. Modified after Konečný et al. (1995).

volcanic magmas sourced from an upper crustal magmatic reservoir that crystallized at pressures between ~1 and ~3 kbar (Rottier et al. 2020).

Structural and metallogenetic evolution

The Štiavnica Stratovolcano as defined by (Konečný et al. 1983, 1998a) is a lithostratigraphic unit at the level of a group, not a stratovolcano in the volcanological sense. In reality it represents a complex/compound volcanic edifice composed of a succession of volcanic/intrusive formations and complexes with common central, proximal and distal zones. It has a long lasting history, including breaks in volcanic/intrusive activity and periods of denudation observed as unconformities. Despite a significant denudation, it still extends over the area of 2200 km^2 (Fig. 2). Characteristic features include: a complex structure involving differentiated rocks, extensive subvolcanic intrusions, a caldera 20 km in diameter and a late-stage resurgent horst associated with a rhyolite volcanic activity. The edifice has a well established geological and structural evolution based on systematic geological mapping. It is summarized by Lexa et al. (1999a) and Chernyshev et al. (2013) so here we report essential aspects only and new findings.

Main structural units of the volcano correspond to five essential stages distinguished in its evolution: (1) formation of the extensive and complex andesite stratovolcanic edifice, (2) emplacement of subvolcanic intrusions and contemporaneous denudation of the edifice (including a sector collapse, Kubač et al. 2018), (3) caldera subsidence and its filling by evolved andesites, (4) renewed activity of less evolved andesites, (5) uplift of the resurgent horst in the central part of the caldera accompanied by rhyolite volcanic/intrusive activity. Most of the Štiavnica Stratovolcano edifice has evolved in a terrestrial environment and volcanic facies grade in the distal zone into volcano-sedimentary complexes laid down variably in ephemeral stream, fluvial, limnic and/or shallow marine environments.

The *lower structural unit* (*1st or pre-caldera stage*) comprises a succession of pyroxene and hornblende–pyroxene andesite stratovolcanic complexes and formations that represent volcanic activity preceding the caldera subsidence. Its evolution was interrupted by periods of quiescence and related erosion separating individual volcanic formations. Paleovolcanic reconstruction points to remnants of a large and complex stratovolcanic edifice, 40 km in diameter at its base, surrounded by accumulations of epiclastic volcanic rocks (Konečný et al. 1995, 1998a, b). In the central zone of the stratovolcanic edifice, the lower structural unit is exposed in

the eastern half of the resurgent horst (Fig. 3). Here, the former stratovolcano has been deeply eroded (but less than in the western part where basement units are exposed) and the lower structural unit is built mostly of pyroxene, amphibole–pyroxene and biotite–amphibole–pyroxene andesite sills and laccoliths emplaced in the lower part of the andesite stratovolcanic complex above the basement rocks.

In the proximal zone (outside of the caldera) the pre-caldera stage stratovolcanic complexes of the lower structural unit include lava flows, sporadic extrusive domes, pyroclastic flow deposits and epiclastic volcanic breccias. Outward they grade into epiclastic volcanic breccias, conglomerates and sandstones of the distal zone. The lower structural unit comprises also some intrusions. Next to the village Beluj at the south there is a stock of biotite–amphibole–pyroxene diorite porphyry (Stage 1b) that hosts a sub-economic *Au-porphyry mineralization* (Bakos et al. 2010; Kozák et al. 2017). In surroundings of the villages Župkov and Prochot at the west there are sills and laccoliths of andesites invaded by stocks of amphibole–pyroxene diorite porphyry that hosts an incipient base metal mineralization.

During the *2nd stage* in the evolution of the Štiavnica Stratovolcano edifice a long-lasting break in volcanic activity, extensive denudation in the central zone of the former stratovolcanic edifice down to a thickness of 500–1000 m, and emplacement of subvolcanic/intravolcanic intrusions took place. Kubač et al. (2018) and Vojtko et al. (2019) revealed that the extensive denudation in the central zone of the edifice was related to a fast resurgent uplift of the granodiorite pluton and associated sector collapse at the SE side of the stratovolcano. A basal low angle detachment/shear zone hosting a *precious/base metal epithermal mineralization* is exposed in mining works of the B. Hodruša ore deposit at the Rozália mine (Fig. 4). Structural relationships indicate that it is younger than granodiorite pluton and rare pre-mineralization quartz-diorite porphyry sills and older than numerous post-mineralization quartz-diorite porphyry sills (Koděra et al. 2005, 2023; Kubač et al. 2018). Evolution of ore veins was controlled by structural evolution of the low angle shear zone.

The *subvolcanic/intravolcanic intrusive complexes* are exposed in the uplifted block of the resurgent horst in the central zone of the Štiavnica Stratovolcano edifice (Figs. 2, 3). The *Hodruša–Štiavnica Intrusive Complex* comprises an older diorite subvolcanic intrusion and a younger granodiorite bell jar pluton showing a flat roof extending over the area of 100 km^2 and outward dipping margins (Fig. 3). Its thickness exceeds 2000 m. The diorite intrusion in the northern part of the intrusive complex shows a W–E orientation. It is a parental intrusion of the *high-sulfidation hydrothermal system of Šobov* (Lexa et al. 1999b). The system is barren, represented by advanced argillic alteration in andesites of the pre-caldera stage (Onačila et al. 1995; Uhlík & Šucha 1997). The granodiorite pluton invaded basement rocks below the volcanic complex using especially sub-horizontal discontinuities in the Mesozoic sedimentary formations above the Variscan crystalline rocks, resulting in the magma emplacement by an underground cauldron subsidence mechanism (Fig. 3). Such emplacement mechanism is supported by results of magnetic anisotropy measurements that imply a sill-like initial stage (Tomek et al. 2014). Three types of mineralization are associated with the emplacement of the granodiorite bell-jar pluton (Koděra et al. 1998, 2004, 2021). At contacts of the pluton with basement carbonate rocks there are *magnetite skarn deposits and occurrences*. In the central part of the pluton, where it has reached the base of volcanic rocks, the pre-caldera stage andesites are affected by extensive *advanced argillic alteration*, while underlying granodiorite hosts a *stockwork/disseminated base metal mineralization*.

Granodiorite to quartz-diorite porphyry dike clusters and small stocks of the *Zlatno Intrusive Complex* are situated at the periphery of the granodiorite pluton and postdate it. Stocks with roof pendants of basement rocks pass upward into dike clusters emplaced in andesite and andesite porphyry of the lower structural unit. At the locality Vysoká–Zlatno coarse-grained granodiorite porphyry passes into porphyritic granodiorite with increasing depth. Intrusions of the Zlatno Intrusive Complex host the *Cu–Au skarn-porphyry type of mineralization* (Koděra et al. 2010 and references therein) represented by 1 deposit and 6 occurrences. Mineralization occurs in those places where the granodiorite porphyries are in contact with basement limestones and dolomites.

Quartz-diorite porphyry sills of the *Banisko Intrusive Complex* invaded major sub-horizontal discontinuities in basement, granodiorite pluton, contact of basement and volcanic complex and overlying andesites/andesite porphyries of the lower structural unit (Figs. 3, 4). Sills in andesites of the lower structural unit occur especially in the area of the sector collapse where they intrude structures of the shear zone – both, low angle faults as well as moderately dipping tension faults (Kubač et al. 2018; Vojtko et al. 2019). With the exception of few thin sills parallel with the roof of the granodiorite that were emplaced before the precious/base metal epithermal mineralization of the shear zone, emplacement of most sills post-dates this mineralization as well as mineralizations associated with the granodiorite pluton. Further eastward the sills pass into moderately outward dipping ring dikes (Figs. 3, 4).

Quartz-diorite porphyry dikes of the *Banisko Intrusive Complex* extend in the western and northern parts of the resurgent horst, outside of the sills extent (Fig. 3). They are mostly thin, either vertical or dipping inward, showing some aspects of cone sheets that originate via hydraulic fracturing by magma injected at a pressure higher than lithostatic. They post-date granodiorite porphyry stocks/dike clusters and quartz-diorite porphyry sills.

The *middle structural unit* (*3rd or caldera stage*) represents the Štiavnica caldera fill and contemporaneous volcanic deposits on slopes of the Štiavnica Stratovolcano edifice. The caldera is not of the explosive type, has 20 km in diameter (Fig. 2) and the extent of its subsidence is estimated at 500 m. It is filled by biotite-amphibole andesite to rare amphibole–biotite dacite dikes, extrusive domes, dome flows, block and ash pyroclastic flow breccias, subordinate pumice tuffs, and

epiclastic volcanic breccias with lacustrine tuffaceous sediments at the base. Epiclastic volcanic rocks and tuffaceous sediments at the base of the caldera filling and underlying andesites of the pre-caldera stage are at the localities Dekýš and Červená Studňa affected by advanced argillic alteration showing typical features of *hot-spring type systems* (Onačila et al. 1995; Lexa et al. 1997). Next to the village Banská Belá andesites of the caldera fill host a barren *high- sulfidation hydrothermal system of Varta* with characteristic advanced argillic alteration (Onačila et al. 1995; Lexa et al. 1997).

The *upper structural unit* (*4th or post-caldera stage*) comprises mafic to felsic andesitic explosive, stratovolcanic and effusive volcanic complexes/formations that represent volcanic

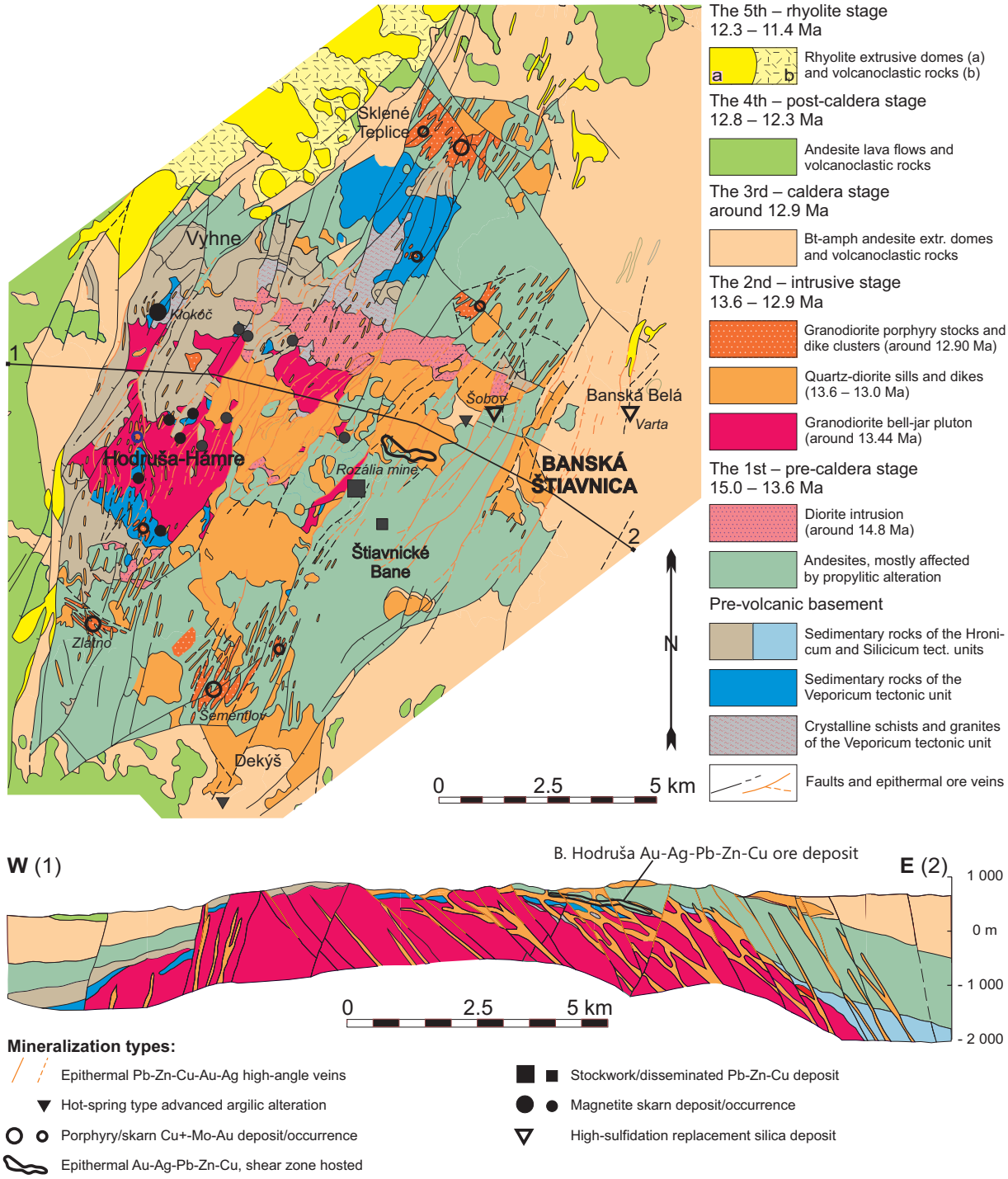

Fig. 3. Structural scheme and section of the resurgent horst in the center of the Štiavnica Stratovolcano caldera with the location of main mineralization types. Modified after Lexa et al. (1999a).

activity postdating the caldera subsidence and pre-dating uplift of the resurgent horst and related rhyolite volcanic activity of the 5th stage (Fig. 2). Individual formations are limited to certain sectors of the stratovolcano with centers in and outside of the caldera. They were often separated by short periods of erosion and filled up radially oriented valleys on slopes of the edifice. At the south, volcanic formations pass into horizons of conglomerates, sandstones and tuffs laid down in a shallow marine environment. No metallogenetic and/or hydrothermal processes are associated with andesite volcanic activity of the post-caldera stage.

The *late-stage rhyolite activity* of *the Jastrabá Fm.* (*5th stage*) created dikes, cryptodomes and extrusive domes on N–S to NE–SW striking faults. In the central zone of the Štiavnica Stratovolcano edifice rhyolite dikes, cryptodomes and extrusive domes follow marginal faults of the resurgent horst, especially at its western and northwestern sides. An extensive dome/flow complex with related pyroclastic and epiclastic rocks spreads along southeastern and eastern marginal faults of the Žiar depression in the northern sector of the stratovolcano (Lexa & Pošteková 2012). The resurgent horst uplift in the central part of the Štiavnica caldera (Fig. 3) was accompanied by an extensive *system of intermediate/low-sulfidation precious/base metal epithermal veins.* Ore veins are localized on faults of the resurgent horst. Their syngenetic erosion and tectonic brecciation point to evolution during the resurgent horst uplift (Kovalenker et al. 1991, 2006; Onačila et al. 1995). The hydrothermal system and rhyolite activity were clearly contemporaneous.

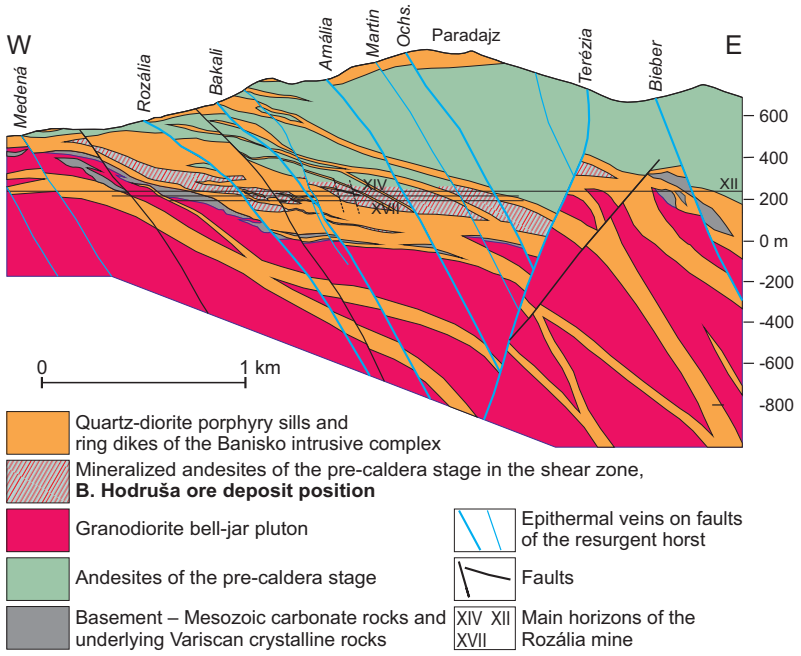

Fig. 4. Schematic section of the B. Hodruša precious/base metal ore deposit at the Rozália mine. Modified after Kubač et al. (2018).

Methodology

SHRIMP U–Th–Pb zircon dating

At least two samples were collected for each of the dated intrusive unit and caldera filling to eliminate accidental errors. Electronic supplement 1 provides their localization and structural position. Individual samples with a mass 1–2 kg were cleaned of surface parts affected by weathering. Samples were subsequently treated by a standard separation method that included crushing, grinding and sieving under 0.5 mesh before hydraulic concentration of heavy minerals on Wilfley table under water stream. Obtained heavy mineral concentrates were subsequently enriched in zircon grains by a separation in bromoform and magnetic separation. Thus, zircon grains finished in a diamagnetic heavy fraction. Zircon grains of similar size were finally handpicked under a binocular microscope, photographed and then mounted in epoxy with FC1 reference zircons (Duluth gabbroic anorthosite, 1099 Ma; Paces & Miller 1993) and SL13 zircon (Sri Lankan gem zircon; U=238 ppm; Roddick & van Breemen 1994). Mounted zircons were grounded till the midsections of samples were exposed and then polished by diamond pastes. Before dating the exposed polished zircon grains were imaged by cathodoluminescence (CL) and back scattered electrons (BSE) using a JEOL 6610LV scanning electron microscope (SEM) at the Korea Basic Science Institute (KBSI) in Ochang. Points for dating in the zircons were selected after control of regular internal structure visible on CL images and the lack of cracks visible on BSE images. U–Pb isotope age of zircons was performed using a SHRIMP IIe/MC ion microprobe housed at KBSI.

Procedures of the SHRIMP analyses were similar to the protocols described in Williams (1998). A 6–8 nA mass filtered O_2-primary beam was focused to a spot of approximately 25 µm diameter on the polished surface of a targeted zircon grain. Each spot was rastered with the primary beam for about 2 minutes prior to the analysis and then analyzed in five cycles with a single electron multiplier. During one cycle, the magnet was stepped through nine peaks of $^{90}Zr_2{}^{16}O$ (counting time =2 s), ^{204}Pb (10 s), ^{206}Pb (20 s), ^{207}Pb (40 s), ^{208}Pb (10 s), ^{238}U (5 s), $^{232}Th^{16}O$ (2 s), $^{238}U^{16}O$ (2 s) and 204.1 (10 s; background position). Counting rates of Pb isotopes were less than 100 counts per second. Despite the increased measurement time of Pb isotopes, due to counting statistics we can not expect a better single spot uncertainty than 5 %. Data processing was conducted using the software SQUID 2.50 (Ludwig 2009) and the weighted means and concordia plots (Electronic supplement 4) were produced using the IsoplotR program (Vermeesch 2018).

Common Pb was removed following the ^{207}Pb correction method using the model by Stacy & Kramers (1975). Weighted mean ages of zircons were calculated using common Pb corrected by assuming a $^{206}Pb/^{238}U$–$^{208}Pb/^{232}Th$ age-concordance, after excluding outliers under statistical t-test to reach reasonable MSWD (cf. Electronic supplement 3) and reported at 95 % confidence. Several samples show clearly a bimodal distribution of single spot ages. In such cases we have calculated separately ages of the older and younger populations of single spot ages (cf. Table 1, Electronic supplement 3). Multiple samples from the same geological unit allowed a calculation of a common/composite isochrone age of the unit based on all measured zircons of the unit. Such common/composite isochrone age we consider as a better estimate of the unit age than the average of individual sample ages. The zircon dating comprises 588 age determination on euhedral and oscillatory zoned zircons (Electronic supplements 2, 3). Points selected for the age determinations are mostly at zircon grains rims, indicated by the numeric code **1** at the end of the grain number, while the inner core positions are indicated by the numeric code **2** at the end of the grain number.

Illite and adularia K/Ar dating

Mineral assemblages of hydrothermal alterations associated with the epithermal mineralization related to a sector collapse of the volcano include illite and adularia. That enabled to date the mineralization by the K/Ar method or to assess the extent of the isotopic system rejuvenation by a younger epithermal mineralization.

The sample collection for this study took place directly in the intermediate-sulfidation precious and base metal deposit Banská Hodruša at the Rozália mine or from underground and surface boreholes (Electronic supplement 1). Information about the mineral composition of altered andesites was obtained from quantitative XRD analyses (Środoń et al. 2001; Eberl 2003). Samples RB-318b and BHS-248/34.5 represent strongly altered andesite with a substantial presence of adularia (72 %, respectively 60 %). Separation of adularia for K/Ar dating was carried out by hand picking under a binocular microscope after gentle grinding. Four illitic samples were separated from intensively argillised andesite with illite (47.2–63.8 wt. %), quartz (18.9–38.6 wt. %) and increased

Table 1: Results of the SHRIMP U–Th–Pb zircon dating on rocks of the Štiavnica Stratovolcano edifice. Reported are concordia ages with errors at the 95 % confidence level calculated using IsoplotR software (Vermeesch 2018) with common Pb corrected by assuming $^{206}Pb/^{238}U$–$^{208}Pb/^{232}Th$ age-concordance.

Stage	Sample	Description		Age (Ma)
1a	BLJ-1	Px andesite porphyry hosting a diorite porphyry stock, Beluj		14.59 ±0.32
1b	BLJ-3	Px-Amph diorite porphyry stock hosting Au-porphyry mineralization, Beluj		14.51 ±0.27
2a	RB-463	Bt-Amph quartz-diorite porphyry sill, pre-mineralization*		13.63 ±0.18
	RB-350	Bt-Amph quartz-diorite porphyry sill, pre-mineralization*		13.58 ±0.12
	RB-463 + RB-350	Pre-mineralization* quartz-diorite porphyry sills		13.60 ±0.10
	RB-1073	Bt-Amph granodiorite bell-jar pluton, Hodruša – Ravenstein		13.43 ±0.14
	RB-1149	Bt-Amph granodiorite bell-jar pluton, Hodruša – All Saints mine		13.49 ±0.16
	GD-1	Bt-Amph granodiorite bell-jar pluton, Hodruša – Mayer shaft		13.36 ±0.13
	RB-1073 + RB-1149 + GD-1	Bt-Amph granodiorite bell-jar pluton		13.44 ±0.08
2b	RB-462	Bt-Amph quartz–diorite porphyry sill, post-mineralization*		13.33 ±0.13
	RB-349	Bt-Amph quartz–diorite porphyry sill, post-mineralization*		13.32 ±0.09
	RB-462 + RB-349	Post-mineralization* quartz-diorite porphyry sills		13.31 ±0.09
	KDP-1	Opx-Bt-Amph andesite porphyry sill, Paradajz		13.62 ±0.23
	RB-1148	Thick Bt-Amph quartz-diorite porphyry sill above the granodiorite pluton, Hodruša		13.19 ±0.13
	KDP-3	Bt-Amph quartz-diorite porphyry ring dike, Juraj adit, Banská Štiavnica		13.04 ±0.12
2c	R-8	Bt-Amph granodiorite porphyry stock; borehole R-8, Vysoká-Zlatno		12.85 ±0.12
	R-12	Bt-Amph granodiorite porphyry stock; borehole R-12, Vysoká-Zlatno		12.92 ±0.09
	R-8 + R-12	Granodiorite porphyry stocks; Zlatno		12.90 ±0.07
	SEM	Bt-Amph granodiorite porphyry thick dike; Šementlov		12.92 ±0.12
	Ti-5	Bt-Amph granodiorite porphyry thick dike; Pukanec		11.81 ±0.17
3	ST-102	Glassy Amph-Bt andesite lava flow, early caldera fill, Ilija		12.99 ±0.16
	ST-104	Amph-Bt andesite extrusive dome; middle caldera fill, north of Močiar	Bimodal population	13.70 ±0.17 13.00 ±0.16
	St-105	Amph-Bt andesite porphyry dike; late caldera fill, northwest of Močiar	Bimodal population	12.89 ±0.17 11.70 ±0.18
	ST-107	Amph-Bt andesite extrusive dome; late caldera fill, south of Močiar		12.90 ±0.09
	St-102, 104 young, 105 old, 107	Amf-Bt andesites of the caldera fill		12.93 ±0.07
5	R-1	Qtz-San-Plg rhyolite cryptodome, Vyhne	Bimodal population	12.46 ±0.10 11.39 ±0.11

Errors are reported as 2 sigma – at a 95 % confidence level

Gray fields are common/composite ages calculated on the basis of zircons from two to four samples of the same unit

* in respect to the B. Hodruša precious/base metal mineralization hosted by the shear zone

concentration of pyrite (3–12 wt. %). Samples were ground to less than 160 μm fraction) and subsequently illite was separated by sedimentation and centrifugation according to the Stokes' law. To verify the presence of large plates of illite over 20 or 50 μm more sodium hexametaphosphate as dispersing agent and ultrasonic bath for a longer time were used to reduce the floculation and aggregation of illite particles during separation. Different size fractions of illitic samples after gold coating were observed by JEOL EVO® 40 Series at the Institute of Inorganic Chemistry of the Slovak Academy of Sciences. Two portions of each sample, a ~30 mg and a ~50 mg, were weighted. A small quantity of CuO (approximately 0.1 mg) was added to the lighter portion. This sample was then wrapped in an Al-foil and subjected to radiogenic argon measurement. The heavier portion was weighted directly on a platinum evaporator and subjected to potassium measurement.

Radiogenic argon measurements were performed on a Nu Instruments Noblesse multicollector noble-gas spectrometer (NG 039). The Al-foil wrapped portions were melted in a double-vacuum resistant crucible at ~1200 °C. Pure ^{38}Ar produced by the Institute for Inorganic and Physical Chemistry of Bern University was used as the spike. CuO added to the samples enhances the oxidation of organic matter during this step. Titanium sponge that acts as a sublimation getter was always put to the place of the reactor where samples are heated. This was a first cleaning level of gases extracted from the samples. The final purification of argon was carried out in an isolated section of the line by a warm getter pump (D-100, SAES Getters), monitored not to release additional argon atoms (after installation it was activated for 12 hrs). Small portions of a gas aliquot released from a sample (ca. 1 %) was then measured at least three times by opening and closing valves of the preparatory line in a specified sequence. Blank measurements were performed every several samples and confirmed that released argon for every sample was above 99.5 %.

Every day, the $^{40}Ar/^{36}Ar$ and $^{40}Ar/^{38}Ar$ ratios are measured for air sample aliquots, delivered from a calibrated air pipette. Based on these results $^{40}Ar/^{36}Ar$ and $^{40}Ar/^{38}Ar$ ratios were corrected for instrument mass fractionation and detector efficiencies assuming atmospheric ratios of $(^{40}Ar/^{36}Ar)_{air}=298.57$ and $(^{40}Ar/^{38}Ar)_{air}=1583.52$ (Lee et al. 2006). The amount of the original aliquot of ^{38}Ar spike was determined by measuring of the international standard GL-O glauconite, performed every day. For this series of samples 1σ for GL-O is 0.7 % (13 samples). Standard age errors were calculated from the law of error propagation also taking these values into account.

The potassium contents were measured using a Sherwood Model 420 flame photometer. The maximum error of this measurement was estimated to be equal 0.03 % K. Based on 6 measurements, K content in GL-O glauconite was slightly higher: 6.61 ±0.02 %, than that of the standard: 6.56±0.06 % (Odin et al. 1982). LP-6 biotite has slightly lower amount of K: 8.27±0.022 % (4 measurements) comparing to the reference value: 8.33±0.03 % (Odin et al. 1982). Both measured standards are within reference ranges assuming 0.03 % K error.

Gold and sulfide Re–Os dating

We have also attempted to date the sector collapse related epithermal mineralization directly by dating gold and sulfides by the Re/Os method. Monomineral separates were prepared from representative samples of all stages of epithermal mineralization at the Rozália mine in Hodruša (Kubač et al. 2018). Samples came from various parts and levels of the mine, collected during the years 2011–2020. Exact position of the samples in the mine including coordinates is in the Electronic supplement 5. Samples with selected sulfides, potentially suitable for the Re–Os dating (pyrite, chalcopyrite), were crushed, sieved and hand-picked using a binocular microscope. For gold-rich samples crushing, milling and wet gravitational concentration was applied. The gold concentrate was macerated in nitric acid, followed by dispersion of precipitates by ultrasound, cleaning of gold by manual panning and in ultrasound, and final cleaning in hydrofluoric acid. In total, 8 pyrite, 7 chalcopyrite and 3 gold monomineral samples were prepared. In order to avoid failure of Re–Os analyses due to a very low Re content, the initial concentration of Re in each sample was checked at the Czech Academy of Sciences. This included decomposition (typically up to 100 mg) of each sample in the presence of ^{185}Re spike (isotopic dilution), equilibration of the solution for ion chromatography, ion chromatography with separation of Re from the matrix, isotopic analysis of Re using SF-ICP-MS and calculation of the Re content.

The Re–Os analyses were performed just on monomineral separates, having suitable amount of Re. 0.75 to 1.5 g samples were digested by the carius tube method (Shirey & Walker 1995) with the addition of hydrogen peroxide to ensure oxidation of samples. Re–Os was extracted through a distillation process similar to that discussed by Frei et al. (1998) and Mathur et al. (2003). Os was further purified by a microdistillation (Roy-Barman et al. 1998), and Re was purified through a two-stage column procedure. Samples were analyzed on a negative thermal ionization mass spectrometer at the University of Arizona; loading and running procedures are highlighted in Chesly & Ruiz (1998). The greatest source of error in our analysis is the concentration of the Os blank ($^{187}Os/^{188}Os=0.22$). Full procedural blanks for this study ranged from 0.4 to 0.9 pg Os and 20 to 30 pg Re. All reported errors on measured values represent the deviation about the mean when the change of the blank is considered.

Results

U–Th–Pb zircon dating

Optical microscopy and BSE images of dated samples imply that zircon grains occur mostly in groundmass of volcanic rock or in interstitial position of holocrystalline intrusive rocks. Less frequently they are enclosed in phenocrysts of

amphibole, biotite or plagioclase (Fig. 5). Usually they associate with apatite, magnetite and/or ilmenite.

Zircons in all dated rock types are transparent, pinkish in color and euhedral (Fig. 6A). Their size is variable, reaching up to 0.5 mm in diameter. Median values of Th/U ratios of dated zircons in samples of Beluj diorite porphyry, granodiorite and pre-mineralization quartz-diorite porphyry vary in the range 0.47–0.54, while those in samples of post-mineralization quartz-diorite porphyry, granodiorite porphyry and caldera filling andesites vary in the range 0.33–0.38. Standard deviation of single zircon values for individual samples varies in the range 0.05–0.17. Th/U ratios of dated rock samples varies in the range 3.39–4.27 with median at 3.78 and standard deviation 0.29 (whole rock analyses are available in an electronic supplement of the paper Rottier et al. 2020). It follows, that a median Th-disequilibrium factor (Th/U mineral / Th/U rock) for individual samples varies in the range 0.10–0.15 with a mode at 0.11 (values for individual zircon grains and median values for individual samples are in the Electronic supplement 3).

CL images in the Fig. 6 and those in the Electronic supplement 2 provide information on morphology and internal structure of dated zircon grains. Simple prismatic crystals dominate over crystals with a more complex morphology. In the sense of Pupin (1980) zircon morphology evolved from prevailing high S morphological subtypes (S25, S20>S24, S19>S23, S18>S22, S17) towards subordinate low S and G subtypes (S5>S4>G), following the trend of calc-alkaline and K-calc-alkaline series according to Pupin (1988). Their elongation varies in the range 1:2 to 1:5 with the average around 1:3. A monotonous oscillatory zoning is the most prominent internal structure (Fig. 6B, C/b,c,d,f,g,h). Fig. 6C/a demonstrates a complete homogenization (a rare section that passed through a single zone cannot be excluded) while Fig. 6C/c,e shows homogenized cores rounded by dissolution. Some of the zircon crystals show a temporal dissolution followed by renewed growth with oscillatory zoning (Fig. 6C/b,c,e,f,h). Resorbed cores are not a frequent feature. Sector zoning (Fig. 6C/g) is rare. Small vacancies occur in crystals with well developed oscillatory zoning (Fig. 6C/c,d,f). Our dating points were measured mostly at rims of grains showing the oscillatory zonality and less frequently at the cores or zones showing homogenization.

Results of SHRIMP U–Th–Pb zircon dating conducted on rocks of the Štiavnica Stratovolcano edifice in the form of interpreted age with 2σ error are in the Table 1. Corresponding

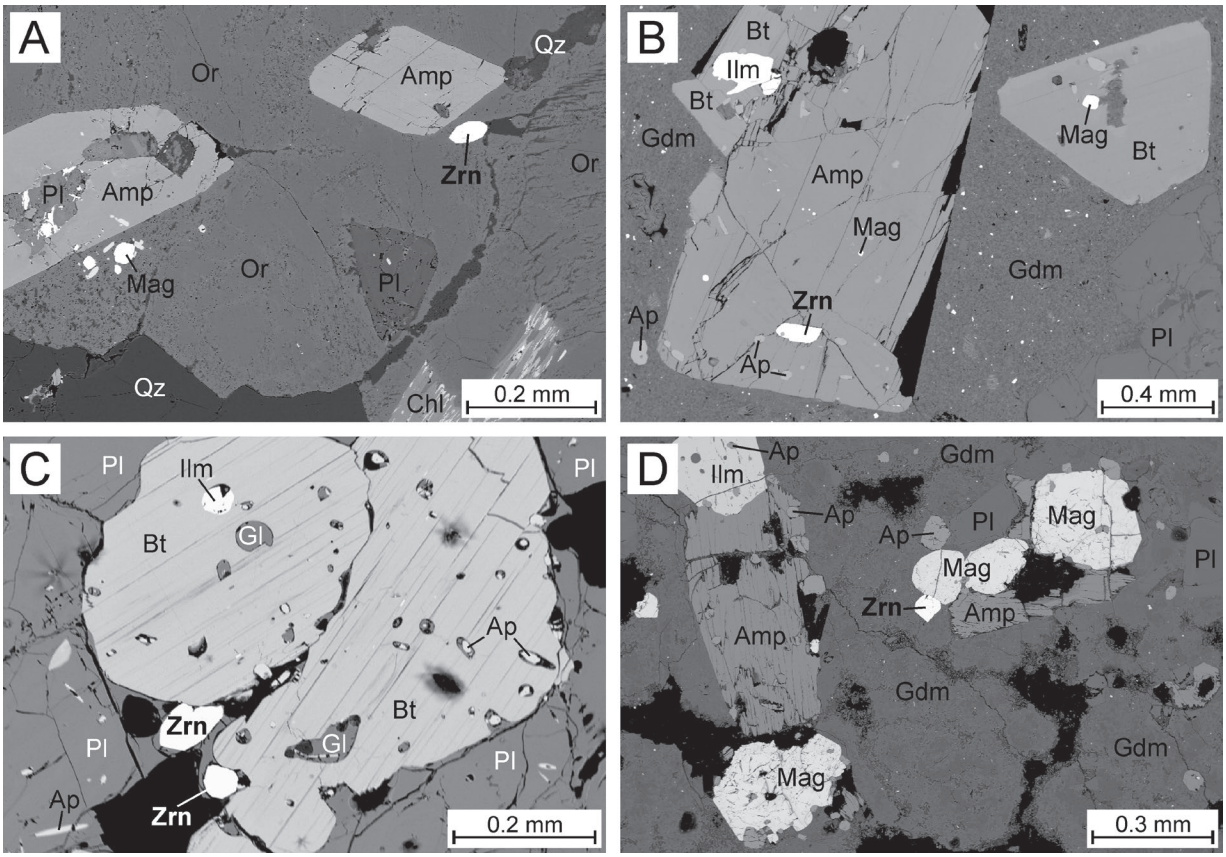

Fig. 5. BSE images showing idiomorphic zircon grains in rocks of the Štiavnica Stratovolcano edifice: **A** — In granodiorite; **B** — Along with ilmenite, magnetite and apatite enclosed in an amphibole phenocryst of amphibole-biotite andesite; **C** — Along with biotite, ilmenite and apatite enclosed in a plagioclase phenocryst of rhyolite; **D** — Along with apatite and microphenocrysts of ilmenite, magnetite, plagioclase and amphibole in groundmass of amphibole-biotite andesite. Mineral symbols are those of Warr (2021), Gdm and Gl stand for groundmass and glass, respectively.

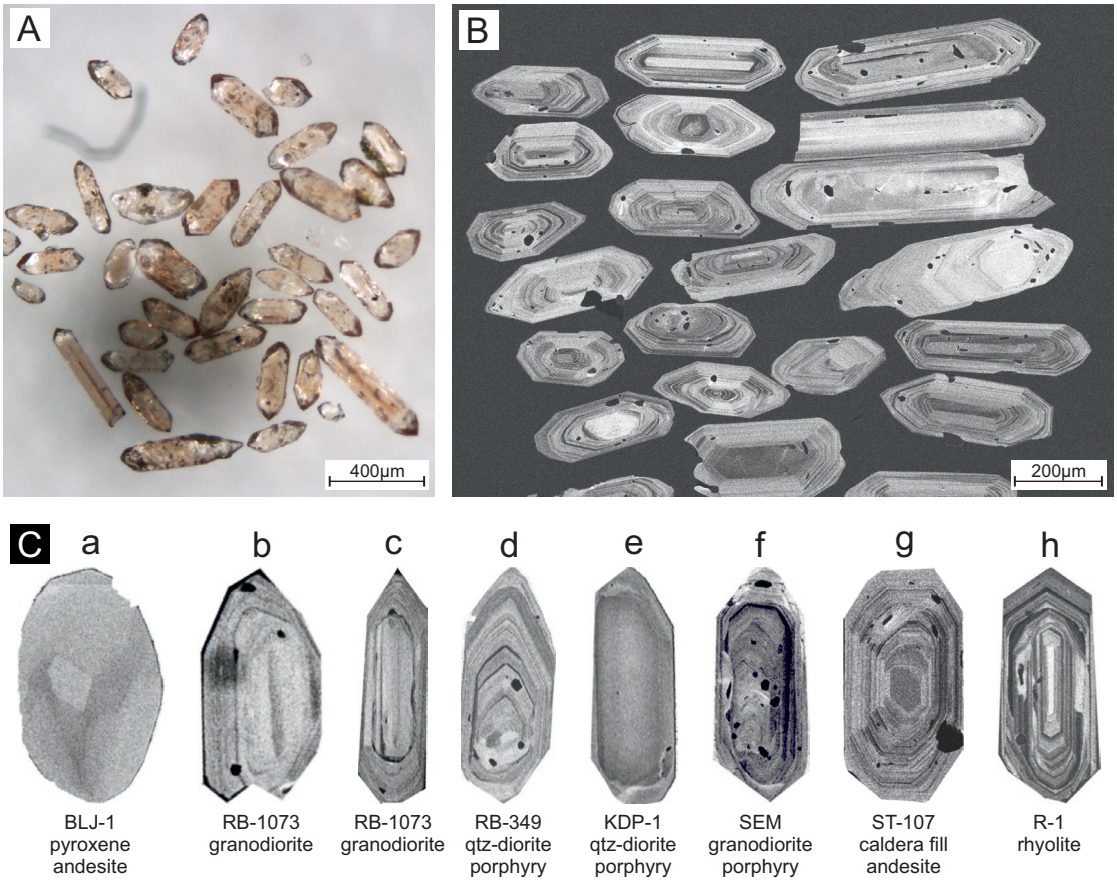

Fig. 6. A and **B** — Micro-photo and CL images, respectively of zircon grains from the sample of quartz-diorite porphyry RB-1148. **C** — The most prominent zircon crystal features, see text for comments.

data tables and concordia plots are in the Electronic supplements 3 and 4. Important events of intrusions emplacement and the caldera subsidence are represented by more than one dated sample. As duration of these events, including the caldera subsidence is shorter than errors of measurements their most probable age can be represented better by calculation of a composite concordia age instead of an average of ages obtained on individual samples (Table 1, Fig. 7).

Illite and adularia K/Ar dating

K/Ar dating has been carried out on 4 samples of illite (one of them split into 3 grain fractions) and on 2 samples of adularia (Table 2). Illite samples were separated from intensively argillised andesite, where it occurs in association with quartz and pyrite. Illite belongs to dioctahedral interlayer-deficient micas with potassium content ranging from 0.65 to 0.86 *apfu* and smectite content smaller than 5 % (Kubač et al. 2018). Clay fractions less than 2 µm show by SEM imaging (Fig. 8) a highly variable size of illite particles. Granular aggregates up to 10 µm in diameter are composed of fine particles with the size less than 1–2 µm (Fig. 8A). Fine particles with the size less than 2 µm also cover the surface of thicker flat particles 50–150 µm in diameter (Fig. 8B). However, XRD and EDS confirmed that illite is a major phase also in coarser fractions composed of thin large flat particles with the size about 100 µm (Fig. 8C). The presence of different sizes of illite particles in clay fraction can be explained by floculation and aggregation during drying or by a real occurrence of large platy particles that are able to float in suspension for a longer time. We should remind that the particle size separation is based on the Stokes' law, and it applies strictly to spherical particles, but not for platy illites (Moore & Reynolds 1997).

The particle size distribution shows relatively homogenous share of fractions (Fig. 9). SEM, however, is not the best tool to distinguish individual particles and scurfs as artefacts after drying. Adularia occurs in adularized andesites as aggregates replacing plagioclase phenocrysts (variably along with sericite), as a network of thin irregular veinlets and/or as aggregates in recrytallized groundmass. In carbonate veinlets it forms typical rombs. Its average Na_2O content is 0.37 wt. % with the maximum at 0.52 wt. % (Kubač et al. 2018).

Gold and sulfides Re/Os dating

A complete presentation of Re/Os isotope data on samples from the Hodruša base/precious metal ore deposit is in the Electronic supplement 5. The analyses of initial concentration

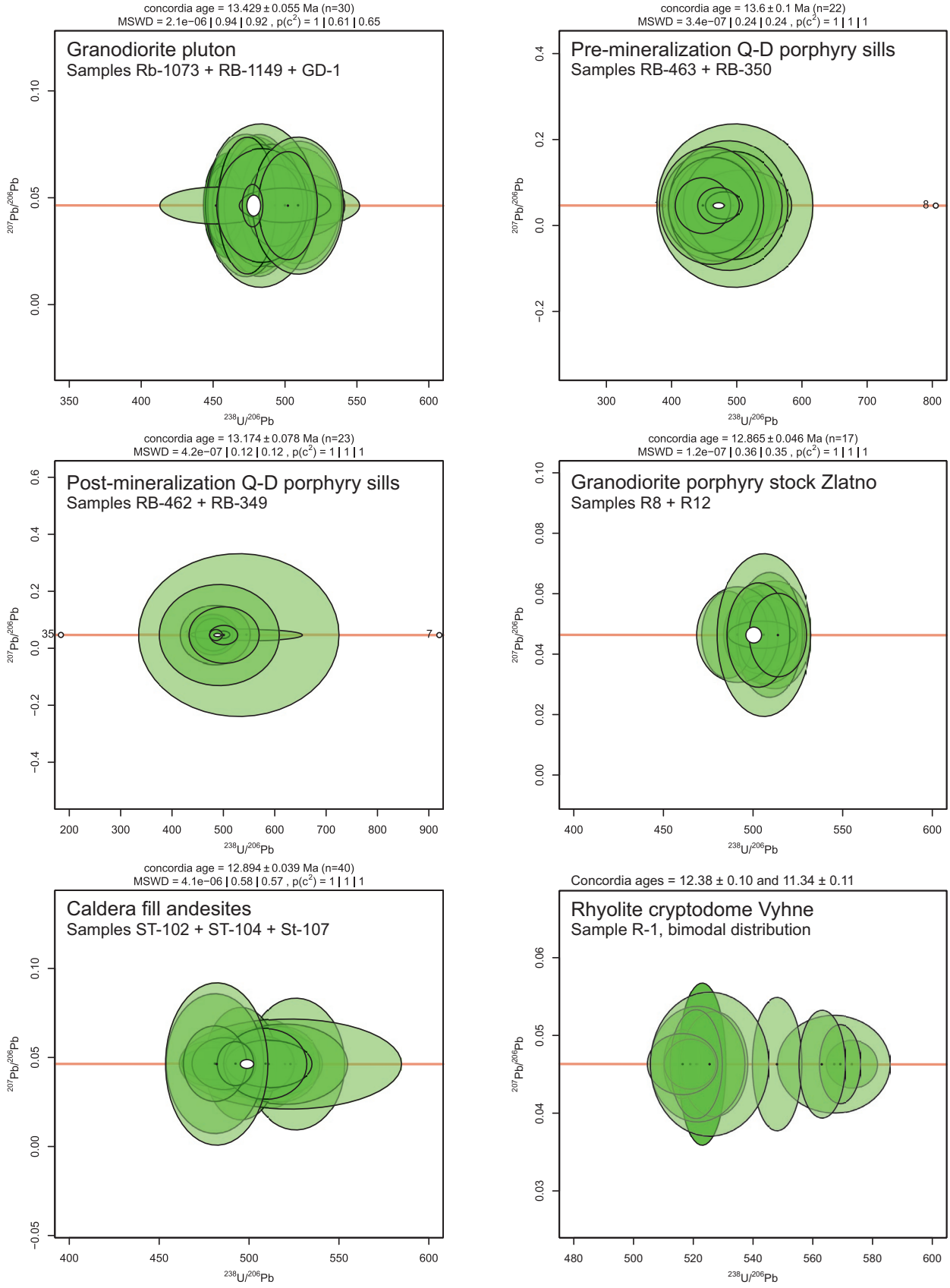

Fig. 7. Composite concordias of subvolcanic intrusion events, caldera fill andesites and a rhyolite sample showing a bimodal zircon population.

Table 2: Results of illite and adularia K/Ar dating, Hodruša ore deposit.

Name	Mass (mg)	K_2O (%)	K (%)	$^{40}Ar^*$ (%)	Age (Ma)	Error (Ma)	Average age (Ma)	Error of average age (Ma)
Illite								
VH-8/156.0 0.2–2 µm Na VH-8/156.0 0.2–2 µm Na	25.70 37.22	7.59	6.30	62.18 58.56	12.28 12.18	0.44 0.45	12.23	0.32
RB-335a 0.2–2 µm Na	32.84	8.73	7.25	71.18	12.77	0.41	12.77	0.41
RB-92a 0.2–2 µm Na RB-92a 0.2–2 µm Na	31.12 30.36	8.63	7.16	71.91 52.78	12.40 12.30	0.39 0.51	12.35	0.32
RB-92a 2–5um RB-92a 2–5um	31.58 21.53	7.21	5.99	61.8 62.9	12.57 12.51	0.46 0.45	12.54	0.32
RB-92a 20–50um RB-92a 20–50um	46.65 32.13	5.39	4.47	63.5 51.9	12.29 12.38	0.45 0.57	12.34	0.36
VH7/72 <2 µm Na VH7/72 <2 µm Na	27.62 32.03	7.90	6.56	71.0 75.5	12.38 12.35	0.44 0.40	12.37	0.30
Adularia								
RB-318b RB-318b	27.81 20.69	11.49	9.53	74.8 71.3	11.86 11.93	0.47 0.53	11.90	0.35
BHS-248/34.5 BHS-248/34.5	31.60 19.79	9.44	7.83	69.1 60.7	12.29 12.43	0.55 0.69	12.36	0.44

of Re in each sample showed very variable Re contents, ranging from 0.3 to 1054 ppb. Thus, the Re–Os isotope analyses were performed just on samples having >0.5 ppb Re, but samples with very high Re contents (>100 ppb) were also omitted, because the high concentrations usually give radiogenic initial values. The samples analyzed for Re–Os isotopic composition contained 2 to 46 ppt Os; however, four of the samples did not have enough Os to measure the isotopes (<0.05 ppt). Re and Os concentrations in the sulfides and gold from the deposit range within previous reported values for similar types of deposits (Mathur et al. 2003; Spry et al. 2013; Kirk et al. 2014; An & Zhu 2018; Liu et al. 2020; Zhao et al. 2020). None of the samples appear to be low level highly radiogenic (LLHR) as defined by Stein et al. (2000). One gold sample and one chalcopyrite sample from an Au-bearing vein have their points on a slope of 13 Ma in the Nicolaysen isochron diagram with an initial $^{187}Os/^{188}Os$ value around 0.2 (Table 3). However not enough data exist to constrain the age with an identified uncertainty, although a long-term well precision of the laboratory, and accuracy of current measurements (2 sigma errors ≤4 %), an overall error propagation can be expected better than ±1.0 Ma. The remaining three pyrite samples and one chalcopyrite do not form a trend in an isochron plot and do not show obvious mixing relationships with the assumed age of 13 Ma. The concentration ranges were low for Os and a total of five repeated attempts to measure Re and Os in different samples of chalcopyrite and native gold failed.

Given that mixing and isochron relationships are not clearly apparent in the studied samples, an attempted robust interpretation of age and source remain more or less elusive. The two data points of gold and chalcopyrite suggest an age congruent with the other mineral geochronology data presented in this publication. The 55 Ma slope (Electronic supplement 5) represents either mixing or is completely meaningless. The radiogenic initial $^{187}Os/^{188}Os$ ratio could indicate that the metals were derived from crustal sources. The initial value is similar to those for other epithermal systems (0.18 to 0.57) that indicate the crustal source input (Mathur et al. 2003; Spry et al. 2013; Kirk et al. 2014; An & Zhu 2018; Liu et al. 2020; Zhao et al. 2020).

Discussion

Reliability of interpreted U–Th–Pb ages

Rocks of the Štiavnica Stratovolcano edifice are a product of a transcrustal magmatic system involving a long-living crystal mush reservoir (Rottier et al. 2020). Zircons represent a common phase of crystal mush that was subsequently mobilized to create a chamber of eruptible magma and thus, if preserved in zircon cores or as inclusions in phenocrysts, they show a relatively older age than the age of magma eruption/emplacement (cf. Miller et al. 2007; Von Quadt et al. 2011; Szymanowski et al. 2017; Cooper 2019). The history of zircon crystal growth, a slow equilibrium growth, a rapid growth from supersaturated melt, recrystallization, multiple growth events, partial dissolution, and inherited cores, are recorded in their morphology and zonality. A generally high elongation of zircon grains, 1 : 3 in average, implies a relatively rapid growth typical for calc-alkaline environment. That is supported by morphology of zircon grains (Fig. 6, Electronic supplement 2) which according to Pupin (1988) follows the calc-alkaline and K-calc-alkaline trend. Most of the zircon crystals show a regular oscillatory zoning formed at the crystal-melt interface during the melt polymerization with a local supersaturation (cf. Clairborne et al. 2010). Loss of magmatic oscillatory zoning and convolute textures result typically

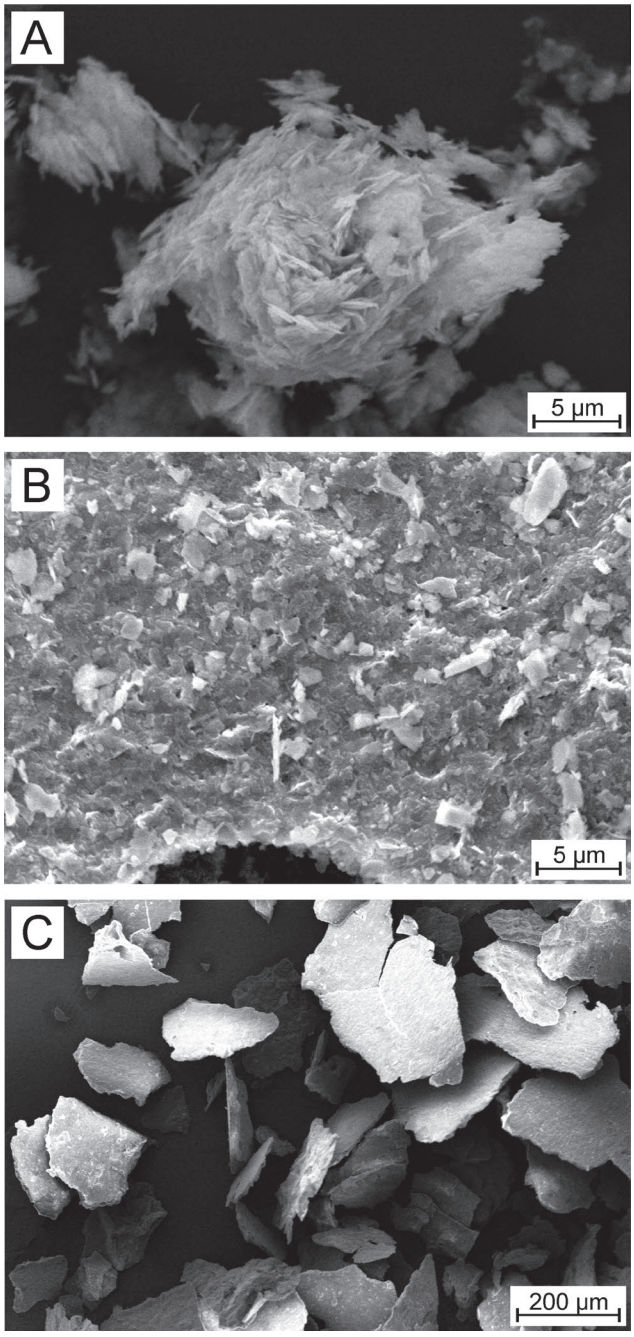

Fig. 8. SEM images of illites from the sample RB-92a (B. Hodruša ore deposit): **A** — Aggregate of illite particles with the size less than 2 µm (fraction <2 µm); **B** — Aggregate of illite particles with the size less than 2 µm (fraction >50 µm); **C** — Large flake-shaped individual particles with size over 50 µm or thin scurf after drying.

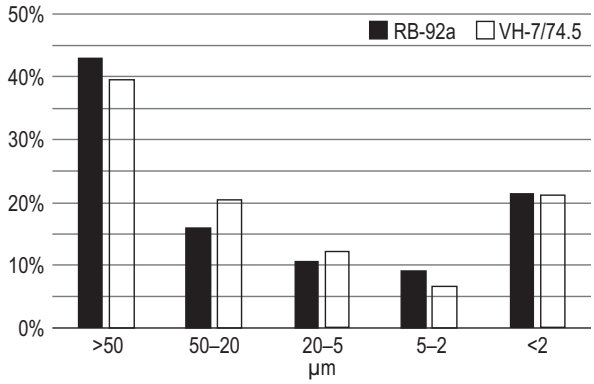

Fig. 9. Particle size distribution of selected samples of illite from the B. Hodruša ore deposit after sedimentation according to the Stokes' law.

from a fluid-mediated regime (cf. Pidgeon 1992; Pidgeon et al. 1998). The crystallization steps indicate a temporary disequilibrium between the zircon and liquid (cf. Martins et al. 2014). Uniform cores represent episodes of slow growth in crystal mush (cf. Hoskin 2000), while resorbed cores represent antecrysts and/or xenocrysts.

Our dating points were measured mostly at rims of grains with well-developed oscillatory zoning, avoiding internal parts that can represent antecrysts, especially if zones of dissolution have been observed. An irregular presence of antecrysts as zircon cores has been actually proven by pairs of dating points measured at the rim and core of single grains, but only a part of cores are unquestionable antecrysts (Fig. 10). However, most of the zircon grains lack obvious cores (Electronic supplement 2), suggesting that the magma was temporarily undersaturated in Zr, probably due to a thermal rejuvenation related to a reservoir recharge event. During required thermal rejuvenation zircon crystals are likely to be at least partially eradicated, however, a complete eradication is also unlikely (Miller et al. 2007). As recorded by monotonous oscillatory zoning, zircon is than assumed to have nucleated homogeneously from melt, saturation being implicitly reached by a drop in temperature (Bouloton 2021). A time interval since mobilization of near-solidus crystal mush into eruptible magma to magma emplacement/eruption is generally very short, on the order of 10–10^4 years (e.g. Cooper 2019). During such a brief interval a significant zircon crystallization or dissolution are unlikely. It follows that interpreted zircon ages based dominantly on spots at grain margins showing the oscillatory zoning represent generally a period of mushy magma crystallization preceding its final mobilization and emplacement. In a situation that uncertainty of single spot measurements exceeds the interval of crystallization as is our case, the length of the interval cannot be resolved (Keller et al. 2018). So, we do not know how much time has really elapsed between the calculated weighted mean concordia age and the age of eruption/ emplacement. However, Tavazzani et al. (2023) on their work concluded that the mass of zircon crystallized in upper crustal magmatic bodies feeding eruptions is not normally distributed, with relatively more zircon mass generated towards the end of the period of crystallization. That, along with a low MSWD weighted mean concordia age calculation (with a preferential removal of relatively older outliers), brings the interpreted age closer to the age of the eruption/ emplacement. This shift towards a slightly older age is at least

Table 3: Results of gold and sulfides Re/Os isochrone dating, Hodruša ore deposit.

Sample	Phase	Re (ppb)	Os (ppt)	$^{187}Re/^{188}Os$	Error	$^{187}Os/^{188}Os$	Error	Isochrone age (Ma)
RB-406	gold	0.891	2	5690	228	1.62	0.06	~13
RB-202b	chalcopyrite	4.6	3	12109	484	2.55	0.10	

* errors represent the deviation about the mean when the change of the blank is considered

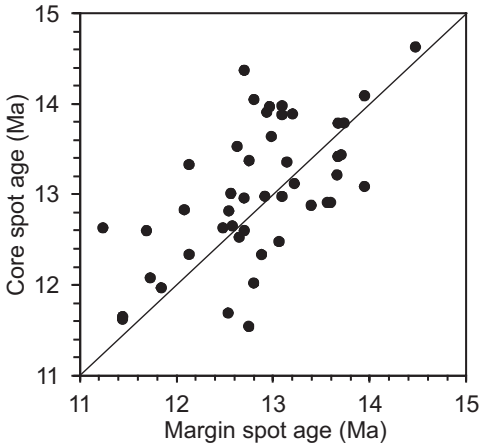

Fig. 10. Confrontation of ages measured at margins and cores of single zircon grains. Data are selected from the Electronic supplement S3. Relatively older zircon grain cores are on the left side of the line.

partially offset by a shift towards a slightly younger age due to the unapplied Th disequilibrium correction (see below). So, our interpreted U–Th–Pb zircon ages should not differ significantly from the age of magma eruption/emplacement.

Dissolution of zircon crystals during thermal rejuvenation does not exclude entirely recycling of zircon antecrysts during successive magmatic injections. That is a primary cause of the modest age dispersion of relevant single spot zircon ages in the case of some samples, and is compatible with a progressive growth of a large, long-lived, crystal mush body (Miller et al. 2007). In our set of dated samples obvious recycling has affected those three samples (ST-104, ST-105, R-1) that show bimodal populations of single spot ages. Three samples show a higher spread of single spot ages (with a higher MSWD) and some age determinations at zircon core spots document the existence of zircon antecrysts and their crystallization up to 1.0 Ma prior to the interpreted age of eruption/emplacement (Fig. 10; Electronic supplement 3). Anyway, to minimize a possible influence of antecrysts on calculated concordia ages, spots showing higher ages were removed preferentially in the process of manual outliers elimination and sporadic older core spot ages were eliminated from the concordia calculations. The bimodal distribution of single spot ages was treated by a separate concordia age calculations for the older and younger populations. Only four out of sixty dated zircon cores are inherited showing ages of the Variscan orogeny (331 Ma) or Cadomian orogeny (561, 613 and 614 Ma, respectively). Apparently, the extent of crustal assimilation was negligible or incorporated zircons were subject to a subsequent dissolution during further evolution of magma in a crustal magma reservoir.

Schärer (1984) pointed to the effect of initial ^{230}Th disequilibrium on young ^{238}U–^{206}Pb ages: "This disequilibrium is due to excess or deficit amounts of radiogenic ^{206}Pb which originate from an excess or deficit of ^{230}Th, respectively, occurring initially in the mineral. Such an initial disequilibrium is caused by the U–Th fractionation between the crystallizing mineral and the magma." Th-poor minerals such as zircon require a correction for a deficit of ^{206}Pb due to a deficiency of ^{230}Th. For rocks with the age 10–15 Ma and Th-disequilibrium factor around 0.11, as there is our case, we can expect a positive correction of the ^{238}U–^{206}Pb ages less than 1 % (Schärer 1984; Bowring et al. 2006). In the Electronic supplement 3 we provide calculated values of the Th-disequilibrium factor for individual zircon grains, median values for individual samples (except those with missing whole rock data) and comparison of the calibrated ^{238}U–^{206}Pb ages accounting for the Th-disequilibrium with ^{238}U–^{206}Pb ages based on common Pb corrected by assuming $^{206}Pb/^{238}U$–$^{207}Pb/^{235}U$ age-concordance. A small relative increase in calibrated ages is not systematic and well within limits of uncertainty. Considering missing data for one third of the samples the application of Th-disequilibrium corrections would disturb relative ages of samples that we consider as more important. However, we are aware that ^{238}U–^{206}Pb ages provided in the Tables 1 and 4 might be generally slightly (less than 1 %) lower in comparison with real ages.

Timing of the Štiavnica Stratovolcano edifice evolution

Essential aspects of the Štiavnica Stratovolcano edifice evolution timing based on 30 K/Ar and 12 Rb/Sr ages of mostly fresh rocks have been laid down by Chernyshev et al. (2013). Discussion concerning age intervals of individual evolutionary stages of the volcano has also considered available biostratigraphic evidence and results of earlier isotope dating by the K/Ar method with references. This method was also used on adularia and illite for dating of hydrothermal processes (Kantor et al. 1985, 1988; Chernyshev at al. 1995, 2000; Kraus et al. 1999; Vlasáč et al. 2024), rhyolites in the Nová Baňa region (Lexa & Pécskay 2010) and high-alumina basalt post-dating rhyolite activity (Balogh et al. 1998). Kohút & Danišík (2017) dated granodiorite and diorite by the U–Th–Pb method on zircon, one sample from each intrusion. In addition they published also (U–Th)/He ages obtained on zircon and apatite from both samples. Electronic supplement 6 provides a summary of previous dating carried out on rocks and

Table 4: Timing of the Štiavnica Stratovolcano edifice evolution – a synthesis of earlier K/Ar and Rb/Sr data with newer U–Th–Pb zircon data. In the right column there are calculated composite U/Pb zircon ages (cc) and on a gray background accepted age intervals interpreted on the basis of discussion in the text.

Stage	Event	Chernyshev et al. (2013) K/Ar and Rb/Sr Interpreted age intervals (Ma)		Other data	Kohút & Danišík (2017) U/Pb zircon (U–Th)/He zircon (Ma)	This work U/Pb zircon (Ma)	This work Interpreted age intervals (Ma)
1a,c	Construction of andesite stratovolcano	15.0–13.5 Isochrone 13.72 ±0.14[1]				14.59 ±0.32	15.0–13.6
1b	Emplacement of the Beluj intrusive complex					14.51 ±0.27	~14.5
1	Emplacement of diorite	13.5–12.9	13.3 ±0.2	Kantor et al. (1988) K/Ar biotite	15.21 ±0.19 14.70 ±0.94		~14.8
2a	Emplacement of pre-ore quartz-diorite porphyry sills					13.63 ±0.18 13.58 ±0.12	cc13.60 ±0.10 ~13.60
	Emplacement of granodiorite		13.4 ±0.2 13.3 ±0.6	13.9 ±0.1	12.92 ±0.27 12.65 ±0.61	13.43 ±0.14 13.49 ±0.16 13.36 ±0.13	cc13.44 ±0.08 ~13.44
2b	Emplacement of post-ore quartz-diorite porphyry sills			Repčok in Chernyshev et al. (2013) 13.4 ±0.6 13.6 ±0.8		13.33 ±0.13 13.32 ±0.09	cc13.31 ±0.09 ~13.31
	Emplacement of other quartz-diorite porphyry sills					13.62 ±0.23 13.19 ±0.13 13.04 ±0.12	~13.6 13.3–13.0
2c	Emplacement of granodiorite porphyry stocks / dike clusters					12.85 ±0.12 12.92 ±0.09 12.92 ±0.12	cc12.90 ±0.07 ~12.9
3	Caldera subsidence and filling	13.1–12.7 Isochrone 12.91 ±0.17[2] 12.87 ±0.05[3]		Lexa & Pécskay (2010) K/Ar (Ma)		12.92 ±0.16 13.00 ±0.16[5] 12.89 ±0.17[4] 12.90 ±0.09	cc12.93 ±0.07 ~12.9
4	Post-caldera andesites	12.7–12.2					12.8–12.3
5	Rhyolites	12.2–11.4		12.31 ±0.44 to 11.52 ±0.36		12.46 ±0.10[4] 11.39 ±0.11[5]	12.3–11.4

[1]isochrone age of 5 K/Ar datings, youngest andesites of the pre-caldera stage (Chernyshev et al. 2013, table 1, no. 8 – 11)
[2]isochrone age of 4 K/Ar datings, andesites of the caldera filling (Chernyshev et al. 2013, table 1, no. 18 – 21)
[3]isochrone age of w.r. – 2 biotites, andesite GK-16 of the caldera filling (Chernyshev et al. 2013, appendix 2, no. 20)
[4]older age, bimodal distribution of single spot ages
[5]younger age, bimodal distribution of single spot ages

mineralizations of the Štiavnica Stratovolcano edifice. Older ones of dubious quality have been discussed by Chernyshev et al. (2013).

Table 4 and Figure 11 show how new U–Th–Pb zircon data fill the gap where K/Ar and Rb/Sr dating could not be applied owing to hydrothermal alteration and possible rejuvenation of isotopic systems. In the right column of the table there are newly interpreted age intervals for the stages in evolution of the Štiavnica Stratovolcano edifice based on a critical evaluation of the past as well as the new data.

Andesites of the *pre-caldera 1st stage* (lower structural unit) comprise a succession of volcanic formations that rest on products of garnet-bearing andesitic volcanic activity (Konečný et al. 1998a). The beginning of the pre-caldera stage andesitic volcanic activity was estimated by Chernyshev et al. (2013; table 2) to around 15.0 Ma. This estimate was based on the biostratigraphic evidence, K/Ar dating of the garnet-bearing andesite to 15.0 ±0.4 Ma and the oldest age on andesite of the pre-caldera stage 14.8 ±0.3 Ma (the dated andesite is not the oldest one in the succession of the pre-caldera stage). Our zircon U–Th–Pb age 14.59 ±0.32 Ma on an andesite lava flow in the middle of the pre-caldera stage succession complies with such a conclusion. The same applies to the age 14.51 ±0.27 Ma of the Beluj intrusive complex that crosscuts older andesites of the pre-caldera stage. Volcanic activity of the pre-caldera stage did not start at the same time in all sectors of the stratovolcano. In the SW sector of the edifice the biostratigraphic evidence from underlying sediments points to a beginning of the pre-caldera stage volcanic activity as late as 14.0 Ma (Chernyshev et al. 2013). The upper limit for volcanic activity of the pre-caldera stage andesites is questionable. Biostratigraphic evidence from overlying sediments and results of K/Ar dating on andesites of a problematic structural position places the upper limit at 13.5–13.2 Ma (Chernyshev et al. 2013). However, isochrone age (IsoplotR, Vermeesch et al. 2018) of five K/Ar datings on andesites of the Žibritov Complex (the youngest in a succession of the pre-caldera stage in the southern sector of the volcano; Chernyshev et al. 2013, table 1, no. 8–11) is 13.72 ±0.14 Ma, while the zircon U–Th–Pb age of the oldest subvolcanic intrusion is around

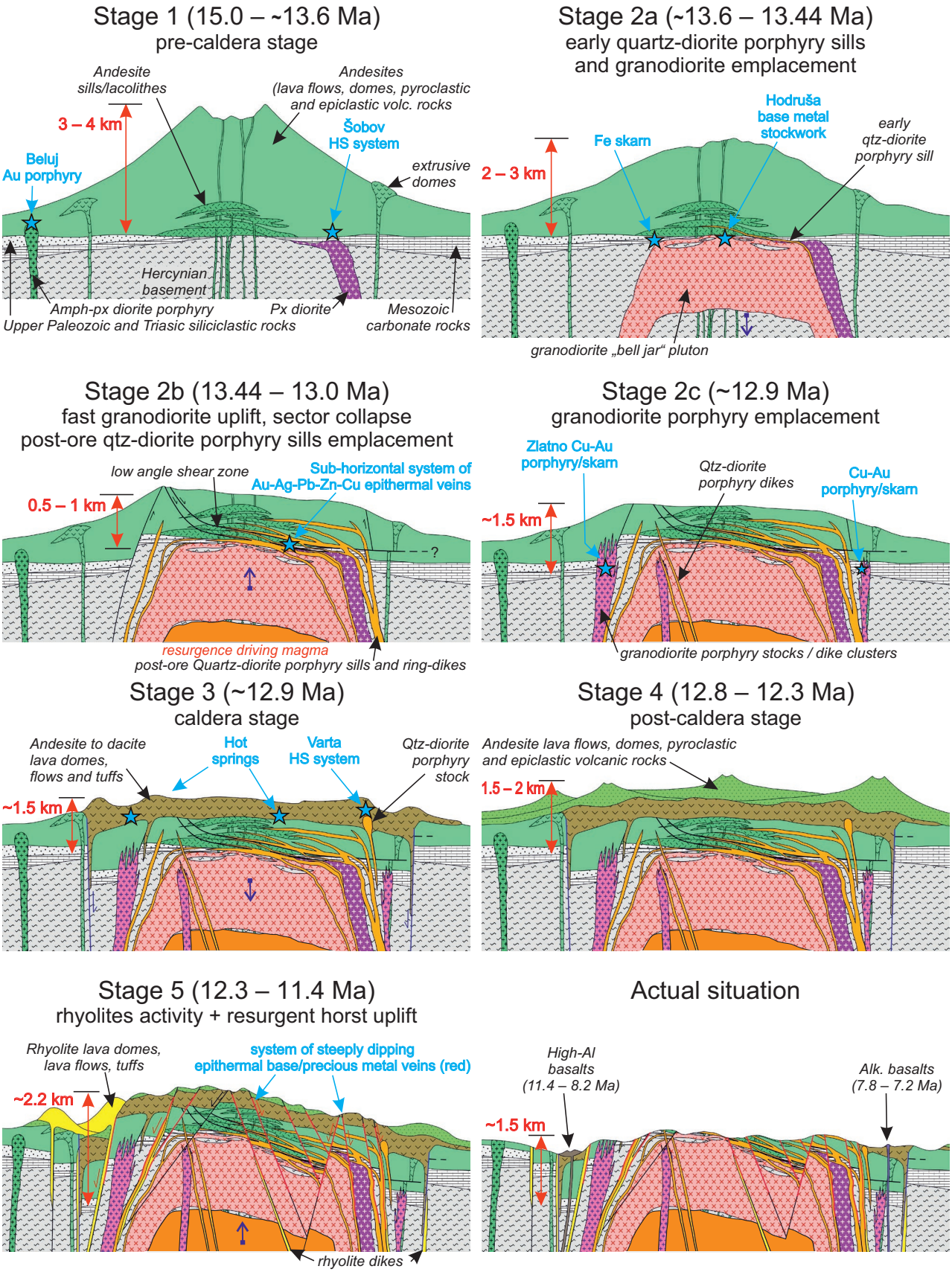

Fig. 11. Evolution of the Štiavnica stratovolcano and associated mineralizations. Modified after Rottier et al. (2020).

13.6 Ma (Table 4; Stage 2a). That places the upper limit of the pre-caldera stage volcanic activity to 13.6 Ma.

The emplacement time of the *diorite intrusion* is problematic. It is older than the granodiorite pluton (~13.44 Ma, Table 4) that shows a magmatic contact with the diorite intrusion (Konečný et al. 1998a). On the other hand, the diorite intrusion is younger than the oldest andesites of the pre-caldera stage as it is in contact with these andesites and a related Šobov high-sulfidation hydrothermal system (diorite is its parental intrusion, see above) is developed in these andesites. It follows that the diorite intrusion should be younger than 15.0 Ma. A direct dating by the Rb/Sr method (Chernyshev et al. 2013) provided a mineral isochron age 13.3±0.2 Ma (Table 4). Such result is not compatible with the age of the granodiorite pluton. Apparently, the Rb/Sr system was rejuvenated by reheating related to the younger hydrothermal system of epithermal veins. Dating of the diorite intrusion by the U–Th–Pb method applied to zircons (Kohút & Danišík 2017) provided an apparent age 15.21±0.19 Ma. This age is not compatible with its structural position (an older age of the pre-caldera stage andesites is not probable). Incorporation of zircons that crystallized in magma prior to its emplacement is a possible explanation (cf. Blundy & Annen 2016; Szymanowski et al. 2017; Cooper 2019). So, we assume that the age of the diorite intrusion emplacement was around 14.8 Ma, close to the age of the oldest andesites of the pre-caldera stage) and compatible with the result of its zircon U–Th/He dating to 14.70±0.94 Ma (Table 4, Kohút & Danišík 2017). Diorite intrusion is not very extensive and 0.1 Ma could be enough to cool down from the emplacement temperature around 900 °C to 200 °C (closing temperature of zircon for the U–Th/He system) following the emplacement into colder rocks.

U–Th–Pb zircon dating of the *Beluj intrusive complex* (Stage 1b) was carried out on biotite–amphibole–pyroxene diorite porphyry hosting the Au-porphyry type mineralization (sample BLJ-3) with a result 14.51±0.27 Ma (Table 4). The age of the intrusive complex around 14.5 Ma is compatible with its structural position as it crosscuts older andesites of the pre-caldera stage and its eroded surface is covered by younger andesites of the pre-caldera stage.

Structural position of the *granodiorite pluton* points to an emplacement age younger than andesites and andesite porphyry of the lower structural unit in the central zone of the stratovolcano (15.0 to 13.6 Ma, see above) and older than most quartz-diorite porphyry sills, including a sill intruded into a contact of granodiorite and pre-caldera stage andesite (U–Th–Pb zircon age 13.19±0.13 Ma, Table 1, sample RB-1148). New U–Th–Pb dating of zircons from three granodiorite samples provided ages 13.43±0.14, 13.49±0.16 and 13.36 ±0.13 Ma with a composite weighted mean age 13.44 ±0.08 Ma. This age is compatible with an older attempt to date emplacement of the granodiorite pluton by the Rb/Sr method. The mineral isochrone ages dominated by biotite are 13.4±0.2 and 13.3±0.6 Ma (Chernyshev et al. 2013, Table 1). However, it is incompatible with the K/Ar dating of biotite to 13.9±0.1 Ma (Kantor et al. 1988). Excess radiogenic argon in biotite is a possible explanation (c.f. Bachmann et al. 2010). In the case of U–Th–Pb zircon dating of granodiorite to 12.92±0.27 Ma (Kohút & Danišík 2017) we do not have a plausible explanation. The granodiorite pluton is quite homogenous, not showing any aspects of a multiple phase emplacement. In summary, we assume that the emplacement of the granodiorite pluton took place around 13.44 Ma.

Quartz-diorite porphyry (QDP) sills and dikes (Stage 2b) were assigned by Konečný et al. (1998a) to the common Banisko intrusive complex, dominantly on the basis of a petrographic kinship. Despite a considerable petrographic variability Konečný et al. (1998a) implicitly assumed emplacement during a relatively short time interval. However, the structural position of the sills is different from the structural position of the dikes. Most of the sills were emplaced by the underground cauldron subsidence mechanism, while the dikes were at least partially emplaced as cone sheets (Konečný et al. 1998a), implying a different state of the magmatic system and related stress field. Also, at the localities Zlatno and Šementlov the QDP sills are crosscut by the granodiorite porphyry (GDP) dikes while at the locality Zlatno the QDP dikes crosscut the GDP dikes (Konečný et. al. 1993, 1998b). At several other localities dikes intruding into sills have been observed. Konečný et al. (1998a) considered the QDP sills and dikes to be older than the caldera fill, allowing for a little overlap at the beginning of the caldera subsidence. Considering interpreted ages of the granodiorite pluton and the caldera fill andesites as well as structural relationships Chernyshev et al. (2013) assigned the QDP sills and dikes of the Banisko intrusive complex to the time interval 13.4–12.9 Ma. FT dating of amphibole and biotite provided results 13.4±0.6 and 13.6±0.8 Ma, respectively (Repčok in Chernyshev et al. 2013). A single K/Ar dating of a sample localized close to one of the younger epithermal veins provided a result 12.5±0.6 Ma (Chernyshev et al. 1995), affected probably by a partial rejuvenation. However, the petrographic variability of QDP sills, as far as the size and proportion of phenocrysts is concerned, points to the variability of the magma source and to probable multiple emplacement episodes. The first geological proof has been observed in the B. Hodruša ore deposit where QDP sills are divided by the mineralization into rare thin "pre-ore" sills affected by the mineralization and prevailing "post-ore" sills that show magmatic contacts with altered andesite hosting the mineralization as well as the mineralization itself (Kubač et al. 2018). Seven new U–Th–Pb zircon datings (Tables 1, 4) confirm these assumptions and findings. They indicate that the QDP sills were emplaced in a succession of events during the time interval ~13.6 to ~13.0 Ma. Results on two samples from the same thin "pre-ore" sill at the B. Hodruša ore deposit are 13.63±0.18 and 13.58±0.12 Ma with a composite weighted mean age 13.60±0.10 Ma pointing to its probable age ~13.6 Ma. Results on two samples from the "post-ore" sills at the Hodruša mine are 13.33±0.13 and 13.32±0.09 Ma with a composite weighted mean age 13.31±0.09 Ma pointing to their age ~13.31 Ma. Results 13.19±0.13 Ma on a sample from the extensive thick

QDP sill in Hodruša and 13.04±0.12 Ma on a sample from a ring-dike in Banská Štiavnica imply that the emplacement of QDP sills/ring dikes continued episodically until ~13.0 Ma. The interpreted age 13.62±0.28 Ma of a sample from a sill at the Paradajz hill points to its relatively early emplacement at a stress field different from the one that controlled emplacement of younger sills (cf. Fig. 4).

Granodiorite porphyry stocks and/or dike clusters (Stage 2c) were considered as generally older than the QDP intrusions of the Banisko intrusive complex on the basis of QDP dikes crosscutting GDP intrusions at the locality Zlatno (Konečný et al. 1998a; Chernyshev et al. 2013). However, as evidenced by geological maps (Konečný et. al. 1993, 1998b), at the localities Zlatno and Šementlov the QDP sills are crosscut by the GDP dikes. Apparently the QDP sills and dikes are not of the same age. Attempts to date GDP emplacement by the K/Ar and Rb/Sr methods were not successful (Chernyshev et al. 1995 and Kráľ et al. 2002) due to rejuvenation by the younger resurgent horst related system of epithermal veins and associated regional propylitization. We have dated three from eight known GDP stocks and/or dike clusters by the U–Th–Pb zircon method. Two samples of different types of GDP at the locality Zlatno provided results 12.85±0.18 and 12.92±0.09 Ma with a composite weighted mean age 12.90±0.07 Ma and GDP at the nearby locality Šementlov provided the age 12.92 ±0.12 Ma. The fourth sample Ti-5 from a thick dike at the locality Hampoch outside of the Štiavnica caldera area shows an interpreted age 11.81±0.17 Ma. Apparently, the rock represents a product of mixing of younger rhyolite magma (see below) with remnants of the granodiorite porphyry type magma represented by the assemblage of phenocrysts, while associated zircons were dissolved. The dike associates spatially with rhyolite dikes (Konečný et. al. 1993, 1998b). Results imply a probable age of the GDP stocks/dike clusters ~12.9 Ma, overlapping with the age of the caldera subsidence. However, we assume that the emplacement of granodiorite porphyry stocks/dike clusters preceded the caldera subsidence (see below). A similar structural position and their common petrography permit a cautious assignment of this age also to the remaining GDP intrusions of the Zlatno intrusive complex.

Previous K/Ar and Rb/Sr dating of the *caldera fill andesites* (3rd stage) and overlying post-caldera stage andesites (4th stage) provided results in the intervals 13.1±0.3 to 12.4 ±0.1 Ma and 13.0±0.3 to 12.0±0.2 Ma, respectively (Chernyshev et al. 2013). Considering overlap of the intervals and available biostratigraphic evidence they assigned the Štiavnica caldera subsidence and it's filling by moderately evolved andesites to the interval 13.1–12.7 Ma. However, the isochrone age (IsoplotR, Vermeesch et al. 2018) of four K/Ar datings on andesites of the caldera filling (Chernyshev et al. 2013, table 1, no. 18–21) is 12.91±0.17 Ma and a mineral Rb/Sr isochrone of the sample GK-16 provided the age 12.9±0.5 Ma (Chernyshev et al. 2013) or12.87±0.05 Ma (MSWD=1.2) if calculated on the basis of whole rock and two biotites using the IsoplotR (Vermeesch et al. 2018). Two (out of four) U–Th–Pb zircon datings of andesites filling the caldera provided results 12.92±0.16 and 12.90±0.09 Ma. The third sample ST-104 that represents an extrusive dome in middle of the caldera filling shows a bimodal distribution of single-spot ages (Electronic supplement 4). The older group of spot ages provides a concordia age 13.70±0.17 Ma, compatible with ages of the oldest subvolcanic intrusions, while the younger group provides a concordia age 13.00±0.16 Ma, compatible with interpreted ages of other andesites in the caldera filling (Table 1). The fourth sample ST-105 that represents a dike crosscutting other andesites of the caldera filling also shows a bimodal distribution of single-spot ages (Electronic supplement 4). The older group of spot ages provides a concordia age 12.89±0.17 Ma, compatible with interpreted ages of other andesites in the caldera filling, while the younger group provides a concordia age 11.70±0.18 Ma, compatible with the age of rhyolites (Table 1). Apparently, the rock represents a product of mixing of younger rhyolite magma (see below) with remnants of the biotite-amphibole andesite or granodiorite porphyry type magma. The dike associates spatially with rhyolite dikes (Konečný et. al. 1993, 1998b). A composite weighted mean age for zircons from the samples ST-102, ST-104 (younger ones), ST-105 (older ones) and ST-107 is 12.93±0.07 Ma (Tables 1, 4, Electronic supplement 4; it is possible to calculate the composite weighted mean age as the caldera formation is a rather rapid process). Taking into account all available data the most probable age of andesites filling the Štiavnica caldera is around 12.9 Ma, overlapping with the age of granodiorite porphyry stocks/dike clusters. Their mutual relationship could not be established exactly, however, we assume that the emplacement of granodiorite porphyry stocks/dike clusters preceded the caldera subsidence that concluded emplacement of subvolcanic intrusions by the underground cauldron subsidence mechanism.

We have no new data on andesites of the Štiavnica Stratovolcano edifice post-caldera stage (4th stage). Chernyshev et al. (2013) obtained results in the interval 13.0±0.3 to 12.0 ±0.2 Ma, however, they put the start of their activity at 12.7 Ma based on the overlap with results on older caldera fill andesites and biostratigraphic evidence for the Early Sarmatian age with the Badenian/Sarmatian boundary at 12.7 Ma (Harzhauser & Piller 2007). However, the age of the older caldera fill andesites has been set to around 12.9 Ma (see above) and the age of the Badenian/Sarmatian boundary has been moved recently to 12.83 Ma (Hohenegger et al. 2014). The post-caldera stage andesites rest on the eroded surface of the caldera fill and the pre-caldera stage andesites outside of the caldera (Konečný et al. 1998a, b). A significant break in volcanic activity is required following the caldera subsidence. It follows that the activity of the post-caldera stage andesites started most probably at around 12.8 Ma. Chernyshev et al. (2013), considering their relationship with younger rhyolites, placed the end of their activity to 12.2 Ma. However, beginning of younger rhyolite volcanic activity is now moved to 12.3 Ma (see below). Summarizing, activity of the Štiavnica Stratovolcano edifice post-caldera stage andesites took place most probably in the interval 12.8–12.3 Ma.

Chernyshev et al. (2013) evaluated eight K/Ar and Rb/Sr datings of the late-stage rhyolites and concluded that their activity took place in the interval 12.2–11.4 Ma (Table 4, Electronic supplement 6). However, K/Ar dating of coeval rhyolites in the Nová Baňa and Kremnica areas by Lexa & Pécskay (2010) (12.31±0.44–12.03±0.38 Ma and 12.29±0.42 –11.52 ±0.36 Ma, respectively; Table 4) extends the interval of rhyolite volcanic activity to 12.3–11.4 Ma. Our new U–Th–Pb zircon dating of a rhyolite cryptodome provides compatible results with a bimodal distribution of individual zircons measurements (cf. Electronic supplement 4) and interpreted ages of 12.46±0.10 and 11.39±0.11 Ma. Apparently, the dated rhyolite emplacement took place at 11.39±0.11 Ma and the presence of older zircons results from the incorporation of antecrysts from a long-living magma reservoir. Considering the upper limit on the age of the post-caldera stage andesites at 12.3 Ma and K/Ar dating of one of the high-alumina basalts post-dating the rhyolite volcanic activity to 11.3±0.80 Ma (Balogh et al. 1998) the interval 12.3–11.4 Ma is the best estimate for activity of the late-stage rhyolites of the Štiavnica Stratovolcano edifice.

Ages of mineralizations hosted by the Štiavnica Stratovolcano edifice

Naturally, mineralizations related to subvolcanic intrusions are of the same age as parental intrusions. The high-sulfidation hydrothermal system of Šobov is probably of the same age as the parental diorite intrusion – around 14.8 Ma. Attempts to date the system by the K/Ar method applied to the $2M_1$ type illite have failed. Results 12.06±0.16 and 11.9±0.37 Ma (Kantor et al. 1985) and 12.4±0.10 Ma (Kraus et al. 1999; Electronic supplement 6) indicate a partial to complete rejuvenation due to reheating by an extensive and long-lasting epithermal system related to the uplift of the resurgent horst (see below a more comprehensive discussion concerning interpretation of similar illite and adularia ages of the precious/base metal epithermal mineralization at the B. Hodruša ore deposit). The Au-porphyry type mineralization at Beluj hosted by a diorite porphyry stock should have an age around 14.5 Ma based on the age of the intrusion. Mineralizations related to the granodiorite pluton (barren advanced argillic and Fe-skarn types) must be of the same age as the pluton – around 13.44 Ma, while the disseminated base metal type is slightly younger, following the pluton solidification. A single K/Ar dating of a sample from the locality Šementlov provided the result 11.4±1.2 Ma (Chernyshev et al. 1995), implying a rejuvenation as in the case of the Šobov hydrothermal system. Au–Cu skarn-porphyry type mineralization hosted by the granodiorite porphyries at Zlatno, Šementlov and Sklené Teplice should have an age around 12.9 Ma. The hot spring type mineralizations at Dekýš and Červená studňa are developed in basal deposits of the Štiavnica caldera implying their age around 12.9 Ma. The high-sulfidation hydrothermal system of Varta next to the village Banská Belá, which is hosted by caldera-fill andesites, is most probably of the same age.

Age of the low-angle shear zone hosted precious/base metal epithermal mineralization at the Hodruša ore deposit is constrained by the U–Th–Pb zircon dating of the "pre-ore" quartz-diorite porphyry sill, granodiorite pluton and "post-ore" quartz-diorite porphyry sills to a rather short 100–150 thousand year long time interval 13.44±0.08–13.31±0.09 Ma (Table 4). We have also attempted to date the mineralization directly by K/Ar method applied to illite and adularia and Re/Os method applied to gold and sulfides. Illite of the $2M_1$>>1M type has been already dated by Kraus et al. (1999) and Chernyshev et al. (2000) with results 11.9±0.3 and 12.8±0.9 Ma, respectively. Our results (Table 2) on illites of various grain size fall in the range 12.72±0.41–12.34 ±0.36 Ma and two results on adularia are 12.36±0.44 and 11.90±0.35 Ma. Identical age of illite for the sample separated into 3 size fractions within errors (RB-92a) indicates that there is no contribution of an older K-bearing mineral, and all minerals contain radiogenic argon closed within the structure in the same period of time. Otherwise there should be differences in the measured age. Taking into account structural position of the mineralization and its age based on U–Th–Pb zircon dating of "pre-ore" and "post-ore" quartz-diorite porphyry sills (see above) the measured illite and adularia ages can not be interpreted as ages of their origin. Temperature of the mineralization has been estimated to 330–270 °C (Kubač et al. 2018) and overlaps with a closing temperature off illite 325–270 °C (Snee at al. 1988), or 350–250 °C (Hueck et al. 2022). That practically excludes a possibility to interpret the measured illite ages as cooling ages. Resetting of ages by a slow process of cooling would also result in relatively older ages of a coarser illite fraction (Hueck et al. 2022) that has not been observed (Table 2). It follows that we are left with the process of partial or complete rejuvenation of illite and adularia ages by the younger epithermal system related to the resurgent horst (its veins crosscut the deposit). Homogenization temperatures of fluid inclusions in minerals of the younger epithermal mineralization point to a temperature interval 335–200 °C with the highest temperatures at the early stages of the mineralization (Kovalenker et al. 2006; Majzlan et al. 2016). Obviously, high enough temperature was reached to open illite and adularia for the K/Ar system rejuvenation. Additionally, a fluid-assisted crystallization re-equilibrates the isotopic system of a mineral much more efficiently than a volume diffusion (Hueck et al. 2022). Identical age for 3 illite size fractions within errors (RB-92a) indicates that all minerals contained radiogenic argon closed within the structure in the same and rather short period of time. Apparently, rejuvenation of illite and adularia ages was incomplete as the age of the younger epithermal system is 12.2–11.4 Ma (see below). Associated regional propylitic alteration indicates that the reheating was not limited just to veins and their surroundings. Thermal rejuvenation is also indicated by (U–Th)/He ages on zircon (T=180–220 °C) and apatite (T=70–120 °C) in granodiorite 12.65±0.61 and 12.26±0.77, respectively (Kohút & Danišík 2017). Re–Os isotopic dating provided a gold–chalcopyrite slope showing the isochrone age around 13 Ma

(Table 3) that is roughly compatible with the age constrained by the U–Th–Pb zircon dating.

The extensive system of intermediate/low-sulfidation precious/base metal epithermal veins is located on faults of the resurgent horst in the central part of the Štiavnica caldera (Fig. 2). Their syngenetic erosion and tectonic brecciation confirm their evolution during the resurgent horst uplift (Kovalenker et al. 1991, 2006; Onačila et al. 1995). Faults of the horst displaced post-caldera stage andesites and were contemporaneous with the emplacement of rhyolites (Konečný et al. 1998a; Chernyshev et al. 2013). Rhyolite dikes often invaded the same faults as the ore veins and are affected by related alterations. So, the activity of rhyolites in the interval 12.3–11.4 Ma suggests a rough time-frame of the ore veins evolution. Next to epithermal veins there are zones of silicification, adularization and argillization with illite as prevailing clay mineral. The K/Ar dating of adularia and adularized rocks has brought ages in the interval 12.11±0.27–10.90±0.20 Ma (Kantor et al. 1985), while the K/Ar dating of the $1M>>2M_1$ type illite provided ages 12.1±0.2 Ma (isochrone age of 4 datings, Chernyshev et al. 1995) and 11.4±0.2 Ma (Kraus et al. 1999). It follows that the resurgent horst-related epithermal system was active for at least 0.7 Ma in the interval 12.2–11.4 Ma with a probable extension for another 0.5 Ma until 10.9 Ma. Such a conclusion is supported by results of adularia and illite K/Ar dating of contemporaneous epithermal systems at Nová Baňa, Rudno, Pukanec and Kremnica in the interval 12.3–11.4 Ma (Electronic supplement 6).

Conclusions

To improve the Štiavnica Stratovolcano edifice timing, especially in the interval of subvolcanic intrusions emplacement and the caldera collapse, we have applied to relevant rocks a precise SHRIMP U–Th–Pb zircon dating, supported by Re/Os gold and sulfide dating and K/Ar adularia/illite dating of the related mineralizations. Zircons show mostly a simple oscillatory zoning with a minimum extent of resorption and/or presence of inherited cores showing Variscan or Cadomian ages. With the exception of three samples (out of 20) showing a bimodal distribution of single spot ages and three samples showing a higher dispersion of single spot ages, the interpreted $^{206}Pb/^{238}U$ concordia ages are reliable, not affected significantly by the presence of antecrysts. Generally, they are compatible with results of previous K/Ar and Rb/Sr dating (Table 4). Their high precision allowed to recognize a succession of subvolcanic intrusions concluded by a caldera collapse (see below). Re/Os gold and sulfide dating of related mineralization provided only one two-point isochrone with an age compatible with the U–Th–Pb dating of pre-mineralization and post-mineralization rocks. K/Ar dating of associated adularia and illite provided only ages rejuvenated by the younger system of epithermal veins. Based on new interpreted age intervals of individual stages and sub-stages in evolution of the Štiavnica Stratovolcano edifice involving a critical evaluation of new and old data (Table 4) we update the scheme of the edifice evolution and related mineralizations (Konečný 1971; Konečný et al. 1983, 1998a; Chernyshev et al. 2013) as follows (Fig. 11): ***Stage 1*** – formation of extensive pyroxene and amphibole–pyroxene andesite stratovolcano during the interval of ca. 15.0–13.6 Ma, including emplacement of a diorite intrusion hosting a barren high sulfidation system at Šobov around 14.8 Ma and emplacement of a diorite porphyry stock at Beluj (***Stage 1b***) hosting the Au-porphyry type mineralization around 14.5 Ma; ***Stage 2*** – emplacement of subvolcanic intrusive rocks and related processes; the stage includes: ***Stage 2a*** – emplacement of quartz-diorite porphyry sills pre-dating the Hodruša epithermal mineralization around 13.6 Ma and emplacement of the granodiorite bell-jar pluton in the depth 2–3 km hosting barren advanced argillic, Fe-skarn and disseminated base metal mineralizations around 13.44 Ma; ***Stage 2b*** – granodiorite pluton resurgent uplift, sector collapse and related evolution of the B. Hodruša precious/base metal epithermal mineralization hosted by a basal shear zone (Kubač et al. 2018; Vojtko et al. 2019) in the interval of ca. 13.44–13.31 Ma; emplacement of quartz-diorite sills in the shear zone that post-date the resurgent uplift and epithermal mineralization around 13.31 Ma; emplacement of other quartz-diorite porphyry sills and ring dikes in broader surroundings of the Hodruša deposit during the interval of ca. 13.3–13.0 Ma; ***Stage 2c*** – emplacement of granodiorite porphyry stocks and dike clusters hosting porphyry-skarn Cu–Au mineralization around 12.9 Ma; ***Stage 3*** – subsidence of the caldera and its filling by evolved amphibole-biotite andesites around 12.9 Ma, including rare hot-spring type siliceous deposits at the base and the barren high-sulfidation epithermal system of Varta; ***Stage 4*** – renewed activity of less evolved pyroxene andesites and mixed type andesites with amphibole and biotite around and in the caldera during the interval of ca. 12.8–12.3 Ma; ***Stage 5*** – uplift of the resurgent horst in the central part of the caldera accompanied by rhyolite extrusive/intrusive activity in the interval of ca. 12.3–11.4 Ma and an extensive system of epithermal precious and base metals veins during the interval of ca. 12.2–10.9 Ma.

Acknowledgements: This study has been carried out in the framework of the grants APVV-15-0083 “Complex model of base and precious metal mineralization at the Rozália mine in Hodruša–Hámre”, VEGA 1/0560/15 “Mineralogy and genesis of economically important types of gold mineralization in the Central Slovakia Volcanic Field” and the grant APVV-SK-KR-18-0008 devoted to a bilateral cooperation with the high resolution ion microprobe laboratory of the Korea Basic Science Institute. M.S. and Z.C. acknowledge NCN (OPUS 2020/37/B/ST10/ 01697) for support of noble gas spectrometer. Cooperation with the Slovenská Banská, Ltd. operating the Hodruša base/precious metal mine is appreciated. We are grateful to anonymous reviewers for their constructive remarks that helped to improve the presentation of our results.

References

An F. & Zhu Y. 2018: Geology and geochemistry of the Early Permian Axi low-sulfidation epithermal gold deposit in North Tianshan (NW China). *Ore Geology Reviews* 100, 12–30. https://doi.org/10.1016/j.oregeorev.2017.03.021

Andrusov D. 1968: Grundriss der Tektonik der nördlichen Karpaten [Basic features of the tectonics of the Northern Carpathians]. *Veda* Verlag, Bratislava, 1–187 (in German with English and Slovak summary).

Annen C., Blundy J.D. & Sparks R.S.J. 2006: The genesis of intermediate and silicic magmas in deep crustal hot zones. *Journal of Petrology* 47, 505–539. https://doi.org/10.1093/petrology/egi084

Bachmann O., Schoene B., Schnyder C. & Spiking R. 2010: The $^{40}Ar/^{39}Ar$ and U/Pb dating of young rhyolites in the Kos-Nisyros volcanic complex, Eastern Aegean Arc, Greece: Age discordance due to excess ^{40}Ar in biotite. *Geochemistry, Geophysics, Geosystems* 11, 1–14. https://doi.org/10.1029/2010GC003073

Bakos F., Fuchs P., Hanes R., Žitňan P. & Konečný V. 2010: Au-porphyry mineralization in the mantle of the Štiavnica Stratovolcano (Western Carpathians). *Mineralia Slovaca* 42, 1–14.

Balogh K., Konečný V. & Lexa J. 1998: K–Ar dating of the youngest calc-alkali rocks in the Central Slovakia Neogene Volcanic Field. *Abstract, XVIth congress CBGA, Vienna*, 59.

Blundy J.D. & Annen C. 2016: Crustal magmatic systems from the perspective of heat transfer. *Elements* 12, 115–120. https://doi.org/10.2113/gselements.12.2.115

Bouloton J. 2021: Origin and significance of volcanic garnet: A detailed petro-mineralogical study of the almandine-bearing andesite of Breziny (Central Slovakia Volcanic Field, Western Carpathians, Central Europe). *Volcanica* 4, 149–187. https://doi.org/10.30909/vol.04.02.149187

Bowring S.A., Schoene B., Crowley J.L., Ramezani J. & Condon D.† 2006: High-precision U–Pb zircon geochronology and the stratigraphic record: progress and promise. In: Olszewski T. (Ed.): Geochronology: Emerging Opportunities, Paleontological Society Short Course, October 21, 2006, Philadelphia, PA. *Paleontological Society Papers* 11, 23–43.

Chernyshev I.V., Háber M., Kovalenker V.A., Ivanenko V.V., Jeleň S. & Karpenko M.I. 1995: To the age position of the magmatic events and epithermal Au–Ag-base metals mineralization in the central zone of the Banská Štiavnica Stratovolcano: K–Ar data. *Geologica Carpathica* 46, 327–334.

Chernyshev I.V., Kraus I., Kovalenker V.A., Goltsman Yu.V. & Lebedev V.A. 2000: Isotope Rb–Sr and K–Ar time constraints for activity of epithermal fluid-magmatic systems: Banská Štiavnica and Kremnica case. *Mineralia Slovaca* 32, 247–248.

Chernyshev I.V., Konečný V. Lexa J., Kovalenker V.A., Jeleň S., Lebedev V.A. & Goltsman Yu.V. 2013: K–Ar and Rb–Sr geochronology and evolution of the Štiavnica Stratovolcano, Central Slovakia. *Geologica Carpathica* 64, 327–351. https://doi.org/10.2478/geoca-2013-0023

Chesley J.T. & Ruiz J. 1998: Crust–mantle interaction in large igneous provinces: implications from the Re–Os isotope systematics of the Columbia River flood basalts. *Earth and Planetary Science Letters* 154, 1–11. https://doi.org/10.1016/S0012-821X(97)00176-3

Clairborne L.L., Miller C.F. & Wooden J.L. 2010: Trace element composition of igneous zircon: a thermal and compositional record of the accumulation and evolution of a large silicic batholith, Spirit Mountain. Nevada. *Contributions to Mineralogy and Petrology* 160, 511–531. https://doi.org/10.1007/s00410-010-0491-5

Csontos L., Nagymarosy A., Horváth F. & Kováč M. 1992: Tertiary evolution of the Intra-Carpathian area: A model. *Tectonophysics* 208, 221–241. https://doi.org/10.1016/0040-1951(92)90346-8

Cooper K.M. 2019: Time scales and temperatures of crystal storage in magma reservoirs: implications for magma reservoir dynamics. *Philosophical Transactionsof the Royal Society A* 377, 20180009. https://doi.org/10.1098/rsta.2018.0009

Eberl D.D. 2003: User's guide to RockJock – a program for determining quantitative mineralogy from powder X-ray diffraction data. *Open File Report 03−78, U.S. Geological Survey*, 1–47. https://pubs.usgs.gov/of/2003/of03-078/

Frei R., Nägle Th.F., Schönberg R. & Kramers J.D. 1998: Re–Os, Sm–Nd, U–Pb, and stepwise lead leaching isotope systematics in shear-zone hosted gold mineralization: genetic tracing and age constraints of crustal hydrothermal activity**.** *Geochimica et Cosmochimica Acta* 62, 1925–1936**.** https://doi.org/10.1016/S0016-7037(98)00111-2

Harangi Sz., Downes H., Thirlwall M. & Gméling K. 2007: Geochemistry, petrogenesis and geodynamic relationships of Miocene calc-alkaline volcanic rocks in the Western Carpathian arc, eastern central Europe. *Journal of Petrology* 48, 2261–2287. https://doi.org/10.1093/petrology/egm059

Harangi Sz., Seghedi I. & Lukács R. 2024: The Neogene to Quaternary Volcanism of the Carpathian–Pannonian Region: from initial plate tectonic models to quantitative petrogenetic explanations. *Geological Society, London, Special Publications* 554 https://doi.org/10.1144/sp554-2024-84

Harzhauser M. & Piller W.E. 2007: Benchmark data of a changing sea – Palaeogeography, palaeobiogeography and events in the Central Paratethys during the Miocene. *Palaeogeography, Palaeoclimatology, Palaeoecology* 253, 8–31. https://doi.org/10.1016/j.palaeo.2007.03.031

Hildreth W. & Moorbath S. 1988: Crustal contribution to arc magmatism in the Andes of Central Chile. *Contributions to Mineralogy and Petrology* 98, 455–489. https://doi.org/10.1007/BF00372365

Hohenegger J., Ćorić S. & Wagreich M. 2014: Timing of the Middle Miocene Badenian Stage of the Central Paratethys. *Geologica Carpathica* 65, 55–66. https://doi.org/10.2478/geoca-2014-0004

Hoskin P.W.O. 2000: Patterns of chaos: fractal statistics and the oscillatory chemistry of zircon. *Geochimica et Cosmochimica Acta* 64, 1905–1923. https://doi.org/10.1016/S0016-7037(00)00330-6

Hueck M., Wemmer K., Ksienzyk A., Kuehn R. & Vogel N. 2022: Potential, premises, and pitfalls of interpreting illite argon dates – A case study from the German Variscides. *Earth-Science Reviews* 232, 104133. https://doi.org/10.1016/j.earscirev.2022.104133

Kantor J., Ďurkovičová J., Eliáš K., Rybár M., Garaj M., Sládková M., Wiegerová V., Rúčka I. & Richtarčik J. 1985: Genetic characteristics of selected mineralizations in Western Carpathians. *Open file report, archive of the D. Štúr State Geological Institute*, Bratislava, 1–138 (in Slovak).

Kantor J., Ďurkovičová J., Eliáš K., Repčok I., Ferenčíková E., Hašková A., Kovářová A., Rúčka I. & Sládková M. 1988: Isotopic research of metallogenetic processes. Part I. The area Rudno–Brehy–Pukanec. *Open file report, archive of the D. Štúr State Geological Institute*, Bratislava, 1–145 (in Slovak).

Keller C.B., Schoene B. & Samperton K.M. 2018: A stochastic sampling approach to zircon eruption age interpretation. *Geochemical Perspectives Letters* 8, 31–35. https://doi.org/10.7185/geochemlet.1826

Kirk J.D., Ruiz J., Kesler S.E., Simon A. & Muntean J.L. 2014: Re–Os age of the pueblo Viejo epithermal deposit, Dominican Republic. *Economic Geology* 109, 503–512.

Kirkland Ch., Smithies R.H., Taylor R.J.M., Noreen E. & Mcdonald B. 2014: Zircon Th/U ratios in magmatic environs. *Lithos* 212–215, 397–414. https://doi.org/10.1016/j.lithos.2014.11.021

Koděra P., Rankin A.H. & Lexa J. 1998: Evolution of fluids responsible for iron skarn mineralisation: An example from the Vyhne-Klokoč deposit, Western Carpathians, Slovakia. *Mineralogy and Petrology* 64, 119–147.

Koděra P., Lexa J., Rankin A.H & Fallick A.E. 2004: Fluid evolution in a subvolcanic granodiorite pluton related to Fe and Pb–Zn mineralization, Banská Štiavnica ore district, Slovakia. *Economic Geology* 99, 1745–1770. https://doi.org/10.2113/gsecongeo.99.8.1745

Koděra P., Lexa J., Rankin A.H. & Fallick A.E. 2005: Epithermal gold veins in a caldera setting: Banská Hodruša, Slovakia. *Mineralium Deposita* 39, 921–943. https://doi.org/10.1007/s00126-004-0449-5

Koděra P., Lexa J. & Fallick A.E. 2010: Formation of the Vysoká–Zlatno Cu–Au skarn–porphyry deposit, Slovakia. *Mineralium Deposita* 45, 817–843. https://doi.org/10.1007/s00126-010-0304-9

Koděra P., Lexa J., Fallick A.E., Wälle M. & Biroň A. 2014: Hydrothermal fluids in epithermal and porphyry Au deposits in the Central Slovakia Volcanic Field. *Geological Society, London, Special Publications* 402, 177–206. https://doi.org/10.1144/sp402.5

Koděra P., Kubač A., Lexa J, Rottier B. & Laurent O. 2021: External controls govern metal endowment and styles of ore mineralisation in andesite volcanoes – example from the Štiavnica stratovolcano, Slovakia. *Proceedings 16th Biennial SGA Meeting* 2, 96.

Koděra P., Lexa J., Chovan M., Vojtko R., Kubač A., Rottier B., Rybárik M. & Prcúch J. 2023: Complex genetic model of the shear-zone hosted epithermal Au–Ag–Pb–Zn–Cu deposit Banská Hodruša at the Rozália mine, Slovakia. *Proceedings 17th Biennial SGA Meeting* 2, 147–150.

Kohút M. & Danišík M. 2017: Rapid cooling and geospeedometry of granitic rocks exhumation within a volcanic arc: A case study from the Central Slovakian Neovolcanic Field (Western Carpathians). *Island Arc* e12201, 11p. https://doi.org/10.1111/iar.12201

Konečný V. 1971: Evolutionary stages of the Banská Štiavnica Caldera and its post-volcanic structures. *Bulletin of Volcanology* 35, 95–116.

Konečný V., Lexa J. & Planderová E. 1983: Stratigraphy of the Central Slovakia Volcanic Field. *Západné Karpaty, sér. Geológia* 9, 1–203 (in Slovak with English summary).

Konečný V., Lexa J. & Hók J. 1993: Geological map of the Štiavnica Stratovolcano central zone 1:10 000 and explanatory notes. *Open file report, archive of the D. Štúr State Geological Institute*, Bratislava, 1–149 (in Slovak).

Konečný V., Lexa J. & Hojstričová V. 1995: The Central Slovakia Neogene volcanic field: a review. In: Downes, H. & Vaselli, O. (eds.): Neogene and related magmatism in the Carpatho–Pannonian region. *Acta Volcanologica* 7, 63–78.

Konečný V., Lexa J., Halouzka R., Hók J., Vozár J., Dublan L., Nagy A., Šimon L., Havrila M., Ivanička J., Hojstričová V., Mihaliková A., Vozárová A., Konečný P., Kováčiková M., Filo M., Marcin D., Klukanová A., Liščák P. & Žáková E. 1998a: Explanations to the geological map of the Štiavnické vrchy and Pohronský Inovec Mountains (Štiavnica Stratovolcano). *Geological Survey of Slovak Republic*, Bratislava, 1–473 (in Slovak with English summary).

Konečný V., Lexa J., Halouzka R., Dublan L., Šimon L., Stolár M., Nagy A., Polák M., Vozár J., Havrila M. & Pristaš J. 1998b: Geological map of the Štiavnické vrchy and Pohronský Inovec Mountains (Štiavnica Stratovolcano) 1:50 000. *The Geological Survey of Slovak Republic*, Bratislava.

Konečný V., Kováč M., Lexa J. & Šefara J. 2002: Neogene evolution of the Carpatho–Pannonian region: an interplay of subduction and back-arc diapiric uprise in the mantle. *EGU Stephan Mueller Special Publication Series* 1, 105–123. https://smsps.copernicus.org/articles/1/105/2002/smsps-1-105-2002.pdf

Kovalenker V.A., Jeleň S., Levin K.A., Naumov V.B., Prokof'ev V.J. & Rusinov V.L. 1991: Mineral assemblages and physical–chemical model of the formation of gold–silver-polymetallic mineralisation on the deposit Banská Štiavnica (Central Slovakia). *Geologica Carpathica* 42, 291–302.

Kovalenker V.A., Naumov V.B., Prokof'ev V.Yu., Jeleň S. & Háber M. 2006: Compositions of magmatic melts and evolution of mineral-forming fluids in the Banska Štiavnica epithermal Au–Ag–Pb–Zn deposit, Slovakia: A study of inclusions in minerals. *Geochemistry International* 44, 118–136. https://doi.org/10.1134/S0016702906020029

Kozák J., Koděra P., Lexa J., Bakos F., Molnár L. & Wälle M. 2017: Porphyry gold system of Beluj in the mantle of the Štiavnica stratovolcano (Slovakia). *Acta Geologica Slovaca* 9, 45–61.

Kraus I., Chernyshev I.V., Šucha V., Kovalenker V.A., Lebedev V.A. & Šamajová E. 1999: Use of illite for K–Ar dating of hydrothermal precious and base metal mineralization in Central Slovak Neogene Volcanic Rocks. *Geologica Carpathica* 50, 353–364.

Kráľ J., Lexa J. & Koděra P. 2002: Isotope geochemistry of the Štiavnica Stratovolcano mineralizations. In: Lexa et al. (eds.): Metallogenetic evaluation of the Slovak Republic territory. *Open file report, archive of the D. Štúr State Geological Institute*, Bratislava, 1–10 (in Slovak).

Kubač A., Chovan M., Koděra P., Kyle J.R., Žitňan P., Lexa J. & Vojtko R. 2018: Mineralogy of the epithermal precious and base metal deposit Banská Hodruša at the Rozália mine (Slovakia). *Mineralogy and Petrology* 112, 705–731. https://doi.org/10.1007/s00710-018-0558-y

Lee J-Y., Marti K., Severinghaus J.P., Kawamura K., Yoo H-S., Lee J.B. & Kim J.S. 2006: A redetermination of the isotopic abundances of atmospheric Ar**.** *Geochimica et Cosmochimica Acta* 70, 4507**–**4512. https://doi.org/10.1016/j.gca.2006.06.1563

Lexa J. & Konečný V. 1988: Geodynamic aspects of the Neogene to Quaternary volcanism. In: Rakús M. (Ed.): Geodynamic development of the Western Carpathians. *Geological Survey of Slovak Republic*, Bratislava, 219–240.

Lexa J. & Pécskay Z. 2010: Radiometric dating of rhyolites by conventional K–Ar method: methodical aspects. In: Kohút M. (Ed.): Dating of minerals and rocks, metamorphic, magmatic and metallogenetic processes, as well as tectonic events. *D. Štúr State Geological Institute*, Bratislava, 21–22.

Lexa J. & Pošteková K. 2012: Eruptive styles of rhyolite volcanoes in the sedimentary basin setting: the case of the Jastrabá Fm. in Central Slovakia. In: Arentsen K., Németh K. & Smid K. (eds.): Fourth International Maar Conference, Auckland, New Zealand, Abstract volume. *Geoscience Society of New Zealand Miscellaneous Publication* 131A, 124–125.

Lexa J., Koděra P., Onačila D., Rojkovičová L., Žáková E. & Trége M. 1997: A complex evaluation of mineral resources in the central zone of the Štiavnica Stratovolcano. *Open file report, archive of the D. Štúr State Geological Institute*, Bratislava, 1–225 (in Slovak).

Lexa J., Štohl J. & Konečný V. 1999a: The Banská Štiavnica ore district: relationship between metallogenetic processes and the geological evolution of a stratovolcano. *Mineralium Deposita* 34, 639–654. https://doi.org/10.1007/s001260050225

Lexa J., Štohl J. & Žáková E. 1999b: The Šobov High-Sulfidation System. In: Molnár F., Lexa J. & Hedenquist J.W. (eds.): Epithermal mineralization of the Western Carpathians. *SEG Guidebook Series* 31, 259–264.

Lexa J., Rottier B., Yi K., Audétat A., Broska I., Koděra P. & Kohút M. 2019: Magmatic evolution of the Štiavnica volcano. In: Proceeding of the Geologica Carpathica 70 Conference. *Earth Science Institute SAS*, Bratislava, 83–86.

Liu Z., Mao X., Ackerman L., Li B., Dick J.M., Yu M., Peng J. & Shahzad S.M. 2020: Two-stage gold mineralization of the Axi epithermal Au deposit, Western Tianshan, NW China: Evidence from Re–Os dating, S isotope, and trace elements of pyrite. *Mineralium Deposita* 55, 863–880. https://doi.org/10.1007/s00126-019-00903-6

Ludwig K. 2009: SQUID 2: A User's Manual. *Berkeley Geochronology Center Special Publication* 5, 1–110.

Majzlan J., Berkh K., Koděra P., Števko M., Bakos F. & Milovský R. 2016: A mineralogical, fluid inclusion, and isotopic study of selected epithermal Ag-Au occurrences in the Banská Štiavnica – Hodruša-Hámre ore district, Western Carpathians. *Acta Geologica Slovaca* 8, 133–147.

Martins H.C.B., Simões P.P. & Abreu J. 2014: Zircon crystal morphology and internal structures as a tool for constraining magma sources: Examples from northern Portugal Variscan biotite-rich granite plutons. *Comptes Rendus Geoscience* 346, 233–243. https://doi.org/10.1016/j.crte.2014.07.004

Mathur R., Ruiz J., Herb P., Hahn L. & Burgath K.P. 2003: Re–Os isotopes applied to the epithermal gold deposits near Bucaramanga, northeastern Colombia. *Journal of South American Earth Sciences* 15, 815–821. https://doi.org/10.1016/S0895-9811(02)00126-8

Miller J.S., Matzel J.E.P., Miller C.F., Burgess S.D. & Miller R.B. 2007: Zircon growth and recycling during the assembly of large, composite arc plutons. *Journal of Volcanology and Geothermal Research* 167, 282–299. https://doi.org/10.1016/j.jvolgeores.2007.04.019

Moore D.M. & Reynolds R.C. Jr. 1997: X-Ray Diffraction and the Identification and Analysis of Clay Minerals. 2nd edtion. *Oxford University Press*, 1–378.

Nemčok M., Pospíšil L., Lexa J. & Donelick R.A. 1998: Tertiary subduction and slab break-off model of the Carpathian–Pannonian region. *Tectonophysics* 295, 307–340. https://doi.org/10.1016/S0040-1951(98)00092-4

Odin G.S. & 35 collaborators, 1982: Interlaboratoiy standards for dating purposes. In: Odin G.S. (Ed.): Numerical Dating in Stratigraphy. *Wiley & Sons*, Chichester, New York, Brisbane, 123–150.

Onačila D., Lexa J., Marsina K., Rojkovičová Ľ., Káčer, Š., Hojstričová V., Žáková E., Štohl J., Konečný V., Nemčok M., Koděra P., Konečný P., Repčok I., Hurai V., Háber M., Jeleň S., Maťo Ľ., Sasvári T., Schmidt R., Zvara I. & Grant T. 1995: Metallogenetic model and resource assesment in the central zone of the Štiavnica Stratovolcano. *Open file report, archive of the D. Štúr State Geological Institute*, Bratislava, 1–231 (in Slovak).

Paces J.B. & Miller J.D. 1993: Precise U–Pb Ages of Duluth Complex and Related Mafic Intrusions, Northeastern Minnesota: Geochronological Insights to Physical, Petrogenic, Paleomagnetic and Tectonomagmatic Processes Associated with the 1.1 Ga Midcontinent Rift System. *Journal of Geophysical Research: Solid Earth* 98, 13997–14013. https://doi.org/10.1029/93JB01159

Pécskay Z., Lexa J., Szakács A., Seghedi I., Balogh K., Konečný V., Zelenka T., Kovacs M., Póka T., Fülöp A., Márton E., Panaiotu C. & Cvetković V. 2006: Geochronology of Neogene–Quaternary magmatism in the Carpathian arc and Intra-Carpathian area: a review. *Geologica Carpathica* 57, 511–530.

Pidgeon R.T. 1992: Recrystallization of oscillatory zoned zircon: some geochronological and petrological implications. *Contributions to Mineralogy and Petrology* 110, 463–472. https://doi.org/10.1007/BF00344081

Pidgeon R.T., Nemchin A.A. & Hitchen G.J. 1998: Internal structures of zircons from Archaen granites from the Darling Range batholith: implications for zircon stability and interpretation of zircon U–Pb ages. *Contributions to Mineralogy and Petrology* 132, 288–299. https://doi.org/10.1007/s004100050422

Pupin J.P. 1980: Zircon and granite petrology. *Contributions to Mineralogy and Petrology* 73, 207–220. https://doi.org/10.1007/BF00381441

Pupin J.P. 1988. Granites as indicators in paleogeodynamics. *Rendiconti – Societa Italiana di Mineralogia e Petrologia* 43, 237–262.

Roddick J.C. & van Breemen O. 1994: U–Pb zircon dating: a comparison of ion microprobe and single grain conventional analysis. In: Radiogenic age and isotopic studies: report 8. *Current Research, Geological Survey of Canada*, 1–9.

Rottier B., Audetat A., Koděra P. & Lexa J. 2020: Magmatic evolution of the mineralized Štiavnica volcano (Central Slovakia): Evidence from thermobarometry, melt inclusions, and sulfide inclusions. *Journal of Volcanology and Geothermal Research* 401, 106967. https://doi.org/10.1016/j.jvolgeores.2020.106967

Roy-Barman M., Wasserburg G.J., Papanatassiou D.A. & Chaussidon M. 1998: Osmium isotopic compositions and Re–Os concentrations in sulfide globules from basaltic glasses: *Earth and Planetary Science Letters* 154, 331–347. https://doi.org/10.1016/S0012-821X(97)00180-5

Seghedi I. & Downes H. 2011: Geochemistry and tectonic development of Cenozoic magmatism in the Carpathian–Pannonian region. *Gondwana Research* 20, 655–672. https://doi.org/10.1016/j.gr.2011.06.009

Schärer U 1984: The effect of initial ^{230}Th disequilibrium on young U–Pb ages: the Makalu case, Himalaya. *Earth and Planetary Science Letters* 67, 191–204.

Shirey S.B. & Walker R.J. 1995: Carius tube digestion for low blank rhenium–osmium analysis: *Analytical Chemistry* 67, 2136–2141.

Snee L.W., Sutter J.F. & Kelly W.C. 1988: Thermochronology of economic mineral deposits – dating the stages of mineralization at Panasqueira, Portugal, by high-precision ^{40}Ar/^{39}Ar age-spectrum techniques on muscovite: *Economic Geology* 83, 335–354. https://doi.org/10.2113/gsecongeo.83.2.335

Spry P., Mathur R., Bonsall T., Voudouris P. & Melfos V. 2013: Re–Os isotope evidence for mixed source components in carbonate-replacement Pb–Zn–Ag deposits in the Lavrion district, Attica, Greece. *Mineralogy and Petrology* 108, 503–513. https://doi.org/10.1007/s00710-013-0314-2

Stacey J. & Kramers J. 1975: Approximation of terrestrial lead isotope evolution by a two-stage model. *Earth and Planetary Science Letters* 26, 207–221. https://doi.org/10.1016/0012-821X(75)90088-6

Stein H.J., Morgan J.W. & Schersten A. 2000: Re–Os Dating of Low-Level Highly Radiogenic (LLHR) Sulfides: The Harnas Gold Deposit, Southwest Sweden, Records Continental-Scale Tectonic Events. *Economic Geology* 95, 1657–1671.

Szymanowski D., Wotzlaw J.-F., Ellis B.S., Bachmann O., Guillong M. & von Quadt A. 2017: Protracted near-solidus storage and pre-eruptive rejuvenation of large magma reservoirs: *Nature Geoscience* 10, 777–782. https://doi.org/10.1038/ngeo3020

Środoń J., Drits V.A., McCarty D.K., Hsieh J.C.C. & Eberl D.D. 2001: Quantitative X-ray diffraction analysis of clay-bearing rocks from random preparations. *Clays and Clay Minerals* 49, 514–528. https://doi.org/10.1346/CCMN.2001.0490604

Tavazzani L., Wotzlaw J.F., Economos R., Sinigoi S., Demarchi G., Szymanowski D., Laurent O., Bachmann O. & Chelle-Michou C. 2023: High-precision zircon age spectra record the dynamics and evolution of large open-system silicic magma reservoirs. *Earth and Planetary Science Letters* 623, 118432. https://doi.org/10.1016/j.epsl.2023.118432

Tomek F., Žák J. & Chadima M. 2014: Magma flow paths and strain patterns in magma chambers growing by floor subsidence: a model based on magnetic fabric study of shallow-level plutons in the Štiavnica volcano–plutonic complex, Western Carpathians. *Bulletin Volcanology* 76, 873. https://doi.org/10.1007/s00445-014-0873-z

Uhlík P. & Šucha V. 1997: Distribution of pyrophyllite in the Šobov deposit and comparison with pyrophyllite from the Vígľašská Huta deposit (Central Slovakia). *Mineralia Slovaca* 29, 73–79.

Vermeesch P. 2018: IsoplotR: A free and open toolbox for geochronology. *Geoscience Frontiers* 9, 1479–1493. https://doi.org/10.1016/j.gsf.2018.04.001

Vlasáč J., Mikuš T., Majzlan J., Števko M., Biroň M., Szczerba M., Milovský R. & Žitňan P. 2024: Mineralogy and evolution of the epithermal mineralization in the Rudno nad Hronom–Brehy ore deposit, Štiavnické vrchy Mts. (Slovakia). *Journal of Geosciences* 69, 21–47. https://doi.org/10.3190/jgeosci.380

Vojtko R., Žitňan P., Prcúch J., Lexa J., Koděra P., Chovan M. & Kubač A. 2019: Structural control of the Banská Hodruša ore deposit (Štiavnica Stratovolcano). In: Proceeding of the Geolo gica Carpathica 70 Conference. *Earth Science Institute SAS*, Bratislava, 45–48.

Von Quadt A., Erni M., Martinek K., Moll M., Peytcheva I. & Heinrich C.A. 2011: Zircon crystallization and the lifetimes of ore-forming magmatic-hydrothermal systems: *Geology* 39, 731–734. https://doi.org/10.1130/G31966.1

Warr L.N. 2021: IMA-CNMNC approved mineral symbols. *Mineralogical Magazine* 85, 291–320. https://doi.org/10.1180/mgm.2021.43

Williams I.S. 1998: U–Th–Pb geochronology by ion microprobe. *Reviews in Economic Geology* 7, 1–35.

Zhao X.Y., Zhong H., Mao W., Bai Z.J. & Xue K. 2020: Molybdenite Re–Os dating and LA-ICP-MS trace element study of sulfide minerals from the Zijinshan high-sulfidation epithermal Cu–Au deposit, Fujian Province, China. *Ore Geology Reviews* 118, 103363. https://doi.org/10.1016/j.oregeorev.2020.103363

Electronic supplementary material is available online:
Supplement 1 at https://geologicacarpathica.com/data/files/supplements/GC-76-Lexa_Suppl1.docx
Supplement 2 at https://geologicacarpathica.com/data/files/supplements/GC-76-Lexa_Suppl2.pdf
Supplement 3 at https://geologicacarpathica.com/data/files/supplements/GC-76-Lexa_Suppl3.xlsx
Supplement 4 at https://geologicacarpathica.com/data/files/supplements/GC-76-Lexa_Suppl4.pdf
Supplement 5 at https://geologicacarpathica.com/data/files/supplements/GC-76-Lexa_Suppl5.xlsx
Supplement 6 at https://geologicacarpathica.com/data/files/supplements/GC-76-Lexa_Suppl6.docx